Developing Analysis, Modeling, and Simulation Tools for Connected and Automated Vehicle Applications

Algorithm Description Document: A Lane Changing Model for Light Duty Connected and Automated Vehicles

August 2020

U.S. Department of Transportation
Federal Highway Administration

Research, Development, and Technology
Turner-Fairbank Highway Research Center
6300 Georgetown Pike
McLean, VA 22101-2296

TECHNICAL REPORT DOCUMENTATION PAGE

<table>
<tr><td>1. Report No.</td><td>2. Government Accession No.</td><td>3. Recipient's Catalog No.</td></tr>
<tr><td colspan="2">4. Title and Subtitle
Developing Analysis, Modeling, and Simulation Tools for Connected and Automated Vehicle Applications Algorithm Description Document: A Lane Changing Model for Light Duty Connected and Automated Vehicles</td><td>5. Report Date
August 2020
6. Performing Organization Code:</td></tr>
<tr><td colspan="2">7. Author(s)
Xiaopeng Li, Qianwen Li, and Zhitong Huang</td><td>8. Performing Organization Report No.</td></tr>
<tr><td colspan="2">9. Performing Organization Name and Address
Leidos Inc.
11251 Roger Bacon Drive
Reston, VA 20190</td><td>10. Work Unit No.
11. Contract or Grant No.
DTFH61-12-D-00030, TO 22</td></tr>
<tr><td colspan="2">12. Sponsoring Agency Name and Address
Office of Operations Research and Development
Federal Highway Administration
6300 Georgetown Pike
McLean, VA 22101-2296</td><td>13. Type of Report and Period Covered
14. Sponsoring Agency Code</td></tr>
<tr><td colspan="3">15. Supplementary Notes
The government task managers were John Halkias and Gene McHale.</td></tr>
<tr><td colspan="3">16. Abstract
This document proposes a new mixed traffic simulation framework that integrates vehicle car-following (CF) and lane-changing (LC) movements in mixed traffic with connected and automated vehicles (CAVs) of different cooperation behaviors. This framework is centered at a CAV LC model integrated with CF dynamics in mixed traffic. The model includes three key components: a CF component, an LC decision-making component, and an LC/LC abortion path generation and following component. Field data were leveraged to demonstrate how to calibrate and validate the proposed CAV model in the mandatory LC context. CAV CF model parameters and safety criterion parameters were calibrated. According to the calibration and validation results, this model's results well replicated the field observations. The proposed mixed traffic simulation framework can be implemented into existing traffic simulators, providing users an opportunity to investigate the impacts of CAV LC and CF on traffic systems and improving the validity of CAV simulation.

This document is also expected to help future users easily adopt and customize this framework in a traffic simulator to meet their simulation needs. To this end, Pseudocode of this framework is included in the appendix.</td></tr>
<tr><td colspan="2">17. Key Words
Connected and automated vehicle, traffic simulation, microsimulation, lane changing, and market penetration rate.</td><td>18. Distribution Statement
No restrictions.</td></tr>
<tr><td>19. Security Classif. (of this report) Unclassified</td><td>20. Security Classif. (of this page) Unclassified</td><td>21. No. of Pages
69
22. Price
N/A</td></tr>
</table>

Form DOT F 1700.7 (8-72) Reproduction of completed page authorized.

SI* (MODERN METRIC) CONVERSION FACTORS

APPROXIMATE CONVERSIONS TO SI UNITS

Symbol	When You Know	Multiply By	To Find	Symbol
		LENGTH		
in	inches	25.4	millimeters	mm
ft	feet	0.305	meters	m
yd	yards	0.914	meters	m
mi	miles	1.61	kilometers	km
		AREA		
in^2	square inches	645.2	square millimeters	mm^2
ft^2	square feet	0.093	square meters	m^2
yd^2	square yard	0.836	square meters	m^2
ac	acres	0.405	hectares	ha
mi^2	square miles	2.59	square kilometers	km^2
		VOLUME		
fl oz	fluid ounces	29.57	milliliters	mL
gal	gallons	3.785	liters	L
ft^3	cubic feet	0.028	cubic meters	m^3
yd^3	cubic yards	0.765	cubic meters	m^3
		NOTE: volumes greater than 1,000 L shall be shown in m^3		
		MASS		
oz	ounces	28.35	grams	g
lb	pounds	0.454	kilograms	kg
T	short tons (2,000 lb)	0.907	megagrams (or “metric ton”)	Mg (or “t”)
		TEMPERATURE (exact degrees)		
°F	Fahrenheit	5 (F-32)/9 or (F-32)/1.8	Celsius	°C
		ILLUMINATION		
fc	foot-candles	10.76	lux	lx
fl	foot-Lamberts	3.426	candela/m^2	cd/m^2
		FORCE and PRESSURE or STRESS		
lbf	poundforce	4.45	newtons	N
lbf/in^2	poundforce per square inch	6.89	kilopascals	kPa

APPROXIMATE CONVERSIONS FROM SI UNITS

Symbol	When You Know	Multiply By	To Find	Symbol
		LENGTH		
mm	millimeters	0.039	inches	in
m	meters	3.28	feet	ft
m	meters	1.09	yards	yd
km	kilometers	0.621	miles	mi
		AREA		
mm^2	square millimeters	0.0016	square inches	in^2
m^2	square meters	10.764	square feet	ft^2
m^2	square meters	1.195	square yards	yd^2
ha	hectares	2.47	acres	ac
km^2	square kilometers	0.386	square miles	mi^2
		VOLUME		
mL	milliliters	0.034	fluid ounces	fl oz
L	liters	0.264	gallons	gal
m^3	cubic meters	35.314	cubic feet	ft^3
m^3	cubic meters	1.307	cubic yards	yd^3
		MASS		
g	grams	0.035	ounces	oz
kg	kilograms	2.202	pounds	lb
Mg (or “t”)	megagrams (or “metric ton”)	1.103	short tons (2,000 lb)	T
		TEMPERATURE (exact degrees)		
°C	Celsius	1.8C+32	Fahrenheit	°F
		ILLUMINATION		
lx	lux	0.0929	foot-candles	fc
cd/m^2	candela/m2	0.2919	foot-Lamberts	fl
		FORCE and PRESSURE or STRESS		
N	newtons	2.225	poundforce	lbf
kPa	kilopascals	0.145	poundforce per square inch	lbf/in^2

*SI is the symbol for International System of Units. Appropriate rounding should be made to comply with Section 4 of ASTM E380. (Revised March 2003)

TABLE OF CONTENTS

EXECUTIVE SUMMARY ... **1**
CHAPTER 1. PURPOSE OF THIS MODEL ... **3**
Purpose of this Document ... 3
Purpose of this Model ... 3
Document Overview ... 5
CHAPTER 2. MODEL DEVELOPMENT AND LOGIC ... **7**
Description of Model Logic ... 7
Connected and Automated Vehicle States ... 9
Connected and Automated Vehicle States ... 9
Connected and Automated Vehicle Lane Changing ... 11
Model Development ... 12
Connected and Automated Vehicle Car-Following Model ... 12
Connected and Automated Vehicle Lane-Changing Model ... 13
CHAPTER 3. MODEL CALIBRATION AND VALIDATION ... **19**
Model Calibration ... 19
Model Validation ... 28
CHAPTER 4. BASIC INFORMATION ON MODEL IMPLEMENTATION ... **35**
CHAPTER 5. USE CASE AND SENSITIVITY STUDY ... **37**
Implementation of the Developed Model into a Traffic Simulation Tool ... 37
Design of Simulation Experiments ... 38
Simulation Results ... 41
Lane-Changing Process Demonstration ... 41
Sensitivity Analysis Results of Congested Traffic ... 42
Sensitivity Analysis Results of Uncongested Traffic ... 50
CHAPTER 6. SUMMARY AND RECOMMENDATIONS ... **59**
REFERENCES ... **61**
APPENDIX – PSEUDOCODE ... **63**
Main Program ... 63
Functions ... 64

LIST OF FIGURES

Figure 1. Flowchart. The proposed mixed traffic simulation framework. 8
Figure 2. Illustration. Vehicle states. 9
Figure 3. Connected and automated vehicle car-following path. 10
Figure 4. Illustration. Uncooperative/cooperative connected and automated vehicle. 10
Figure 5. Illustration. Incentive and safety criteria. 12
Figure 6. Equation. Linear adaptive cruise control model. 12
Figure 7. Equation. Incentive criterion. 13
Figure 8. Equation. Gipps' safe distance. 14
Figure 9. Equation. Target acceleration calculated by intelligent driver model. 14
Figure 10. Equation. A sin-function-based lane-changing path. 15
Figure 11. Equation. A linear function lane-changing path. 15
Figure 12. Illustration. Connected and automated vehicle lane changing/lane-changing abortion path. 16
Figure 13. Illustration. Car following of lane changing. 16
Figure 14. Illustration. Car following of lane-changing abortion. 17
Figure 15. Flowchart. Connected and automated vehicle mandatory lane-changing logic with key parameters. 20
Figure 16. Equation. Root mean square error of the connected and automated vehicle longitudinal positions in model calibration. 21
Figure 17. Equation. The error between the calibrated lane-changing time point and field-observed lane-changing time point in model calibration. 21
Figure 18. Equation. The calibration optimization objective. 22
Figure 19. Equation. Root mean square error of the connected and automated vehicle speeds in model calibration. 22
Figure 20. Graph. Calibration objective function convergence. 23
Figure 21. Graph. Calibration results of case 1. 25
Figure 22. Graph. Calibration results of case 2. 26
Figure 23. Graph. Calibration results of case 3. 27
Figure 24. Graph. Calibration results of case 4. 28
Figure 25. Equation. Root mean square errors of the connected and automated vehicle longitudinal positions and speeds in model validation. 28
Figure 26. Graph. Validation results of case 1. 30
Figure 27. Graph. Validation results of case 2. 31
Figure 28. Graph. Validation results of case 3. 32
Figure 29. Graph. Validation results of case 4. 33
Figure 30. Illustration. The mixed traffic simulation framework implementation. 35
Figure 31. Screenshot. Study road segment. 38
Figure 32. Equation. The connected and automated vehicle average speed. 38
Figure 33. Equation. The connected and automated vehicle speed standard deviation. 39
Figure 34. Equation. The human-driven vehicle average speed. 39
Figure 35. Equation. The human-driven vehicle speed standard deviation. 40
Figure 36. Equation. The average speed across all vehicles. 40
Figure 37. Equation. The speed standard deviation across all vehicles. 40
Figure 38. Screenshots. Connected and automated vehicle lane-changing process. 42

Figure 39. Graph. Sensitivity analysis on connected and automated vehicle penetration rate under congested traffic. 44
Figure 40. Graph. Sensitivity analysis on connected and automated vehicle cooperation rate under congested traffic. 46
Figure 41. Graph. Sensitivity analysis on incentive criterion threshold under congested traffic. 48
Figure 42. Graph. Sensitivity analysis on incentive criterion bias under congested traffic.......... 50
Figure 43. Graph. Sensitivity analysis on connected and automated vehicle penetration rate under uncongested traffic. 52
Figure 44. Graph. Sensitivity analysis on connected and automated vehicle cooperation rate under uncongested traffic. 53
Figure 45. Graph. Sensitivity analysis on incentive criterion threshold under uncongested traffic. 55
Figure 46. Graph. Sensitivity analysis on incentive criterion bias under uncongested traffic...... 56

LIST OF TABLES

Table 1. Calibration results summary. 23
Table 2. Parameters calibration results. 24
Table 3. Validation results summary. 29

LIST OF ABBREVIATIONS

CAV	connected and automated vehicle
USDOT	United States Department of Transportation
AMS	analysis, modeling, and simulation
FHWA	Federal Highway Administration
LC	lane changing
SH	speed harmonization
CM	coordinated merge
CACC	cooperative adaptive cruise control
ACC	adaptive cruise control
HV	human driven vehicle
CF	car following
IDM	intelligent driver model
RMSE	root mean square error
STD	speed standard deviation

EXECUTIVE SUMMARY

This document proposes a new mixed traffic simulation framework that integrates vehicle car-following (CF) and lane-changing (LC) movements in mixed traffic with connected and automated vehicles (CAVs) of different cooperation behaviors. This framework is centered at a CAV LC model integrated with CF dynamics in mixed traffic. The model includes three key components: a CF component, an LC decision-making component, and an LC/LC abortion path generation and following component. When a CAV is at CF state, it can be either cooperative or uncooperative. If the CAV is cooperative, it yields to other CAV LC behaviors; otherwise, it does not yield. This cooperative behavior helps to facilitate lane changes. Incentive and safety criteria were formulated to model both mandatory and incentive-based LC behaviors. An LC abortion module is activated whenever the safety criterion fails to be met before the CAV passes the lane marking. Field data were leveraged to demonstrate how to calibrate and validate the proposed CAV model in the mandatory LC context. CAV CF model parameters and safety criterion parameters were calibrated. According to the calibration and validation results, this model's results well replicated the field observations. The proposed mixed traffic simulation framework can be implemented into existing traffic simulators, providing users an opportunity to investigate the impacts of CAV LC and CF on traffic systems and improving the validity of CAV simulation.

A use case is conducted on an I-75 roadway segment in a traffic simulator where the proposed CAV control logic is used to control CAVs and the traffic simulator default vehicle control rules are used to control HVs. The case study drew a set of managerial insights into how different parameter settings impact the traffic performance including mobility and traffic stability, accounting for uncertain and varying technologies in the process of following CAV deployment. For example, it is noted that the impacts of several key parameters (e.g., CAV cooperation levels and their propensity to make discretionary LCs) on traffic performance are nonlinear (e.g., first improving and then degrading). These findings indicate that efforts may be taken to optimize these parameters from the perspective of transportation operators (e.g., facilities and policies to promote vehicle cooperation) and automakers (e.g., tuning parameters in their LC models) for the best traffic performance. These insights may help stakeholders better understand and prepare for near-future mixed CAV traffic with different LC behaviors, and also suggest the optimal LC configurations for automakers to achieve the best overall traffic performance.

Considering uncertain technology developments and unknown behaviors in emerging mixed traffic, the proposed framework is meant to be adaptable to more general scenarios other than those presented in this study. For example, this study only used the linearized ACC CF model, which can be easily replaced with other customized CF models (e.g., CACC, platooning) per application requirements. Further, this study used the default HV behavior models obtained from the existing pure HV traffic, which may vary in emerging mixed traffic. In the cases that HV exhibit different driving behaviors while interacting with CAVs, the new HV behavior models can be used instead of the default ones in this framework.

This document is also expected to help future users easily adopt and customize this framework in a traffic simulator to meet their simulation needs. To this end, Pseudocode of this framework is included in the appendix.

This research has been performed under a FHWA project entitled “Developing Analysis, Modeling, and Simulation Tools for Connected and Automated Vehicle Applications” (contract number: DTFH6116D00030-0022). To get more information of this FHWA project, readers are encouraged to reference the final project report of this project (Lu et al, forthcoming). This report is under FHWA publication process and it will be available soon.

CHAPTER 1. PURPOSE OF THIS MODEL

PURPOSE OF THIS DOCUMENT

Connected and automated vehicle (CAV) technologies offer potentially transformative societal impacts, including significant mobility, safety, and environmental benefits. State and local agencies are interested in harnessing the potential benefits of CAVs. However, for agencies to be able to plan beneficial deployments of infrastructure-to-vehicle (I2V) and vehicle-to-vehicle (V2V) technology, it is important to be able to robustly predict the impacts of such deployments and identify which applications best address their unique transportation problems. Traffic analysis, modeling, and simulation (AMS) tools provide an efficient means to evaluate transportation improvement projects before deployment.

However, current AMS tools are not well suited for evaluating CAV applications due to their inability to represent vehicle connectivity and automated driving features. The development of a new generation of tools involves spending a lot of resources and time to develop, calibrate, and validate. Many independent researchers have developed models of CAV systems based on a divergent array of underlying assumptions. As a result, there is little consensus in the literature regarding the most likely impacts of CAV technologies.

Thus, there is a desire for a consistent set of models to produce realistic and believable predictions of CAV impacts. These models can be based on the best available data and include the most accurate possible representations of the behaviors of drivers of conventional vehicles and CAVs. Deployment concepts, strategies, and guidelines are also key for allowing State and local agencies to understand how and where to deploy CAV technologies.

To meet these goals, the Federal Highway Administration (FHWA) sponsored a project entitled ‘Developing Analysis, Modeling, and Simulation Tools for Connected and Automated Vehicle Applications’ (contract number: DTFH6116D00030-0022). This project aimed to develop AMS models for the most prominent CAV applications and to incorporate these models into existing AMS simulation tools. Three CAV applications were developed under this project: a lane changing (LC) model for light duty CAVs, a combined application model that integrates speed harmonization (SH) and coordinated merge (CM), and an improved cooperative adaptive cruise control (CACC) model for light duty CAVs.

This document presents a LC model for light duty CAVs in detail. The objective of this document is to provide detailed information of this model to improve the CAV simulation capabilities. This document is expected to help future users easily adopt and customize this model in a traffic simulation tool to meet their simulation needs. To this end, this document describes the algorithms/logics of this model in detail. It also illustrates how this model was developed, calibrated, and validated. Pseudocode of this model is included in the appendix.

PURPOSE OF THIS MODEL

CAV technologies can significantly improve traffic safety and reduce traffic congestion. The Society of Automotive Engineers defines six distinct levels of automated control; with each increasing level, the human driver cedes more control of the vehicle to the automated system

(Smith, 2013). Level 1 automation is defined as when the system can handle longitudinal control of the vehicle under certain conditions and is available in many vehicles today (e.g., ACC on freeways) (Gunter et al., 2019; Xiao and Gao, 2010). LC control is a fundamental leap from Level 1 to higher levels of automation, i.e., SAE Levels 2–5 (Smith, 2013). Thus, to robustly model the impacts of higher levels of automation, analysts and researchers desire accurate models of CAV LC.

Existing studies of LC control are limited to static motion planning without considering surrounding HV dynamics in a mixed traffic environment (Li et al., 2018; Xu et al., 2012). In addition, motion planning and LC decision are separately studied in a static setting. However, these two components are interdependent in real-world driving. Vehicle motions may change dynamically and consequentially affect the LC decision. More importantly, there lacks a comprehensive modeling framework that incorporates both longitudinal and lateral movements of CAVs across different cooperation classes in a mixed traffic environment. Without such a framework, traffic operators and transportation planners may not fully understand or be well prepared for the impacts of CAV LC behaviors in near-future mixed traffic. Further, without this framework bridging an individual vehicle's behavior to system performance, there will remain a gap between automakers that purely focus on an individual vehicle's functions and transportation stakeholders concerned with transportation system performance.

Motivated by the above research gaps, this study proposed a new mixed traffic simulation framework that integrates vehicle CF and LC movements in mixed traffic with CAVs of different cooperation behaviors. This framework is centered at a CAV LC model integrated with CF dynamics in mixed traffic. The model includes three key components: a CF component, an LC decision-making component, and an LC/LC abortion path generation and following component. The research team formulated incentive and safety criteria to model both mandatory and incentive-based LC behaviors. An LC abortion module is activated whenever the safety criterion fails to be met before the CAV passes the lane marking. Field data (Wang et al., 2020) were leveraged to demonstrate how to calibrate and validate the proposed CAV model in the mandatory LC context. According to the calibration and validation results, this model's results well replicated the field observations. To demonstrate the applicability of the proposed model, the team further implemented a case study of a segment of the I–75 freeway in the Tampa Bay area on the Vissim microsimulation platform (PTV Group, 2018). The case study also drew a set of managerial insights into how different parameter settings impact the traffic performance including mobility and traffic stability, accounting for uncertain and varying technologies in the process of following CAV deployment. For example, it is noted that the impacts of several key parameters (e.g., CAV cooperation levels and their propensity to make discretionary LCs) on traffic performance are nonlinear (e.g., first improving and then degrading). These findings indicate that efforts may be taken to optimize these parameters from the perspective of transportation operators (e.g., facilities and policies to promote vehicle cooperation) and automakers (e.g., tuning parameters in their LC models) for the best traffic performance. These insights may help stakeholders better understand and prepare for near-future mixed CAV traffic with different LC behaviors, and also suggest the optimal LC configurations for automakers to achieve the best overall traffic performance.

Considering uncertain technology developments and unknown behaviors in emerging mixed traffic, the proposed framework is meant to be adaptable to more general scenarios other than those presented in this study. For example, this study only used the linearized ACC CF model (Milanés and Shladover, 2014), which can be easily replaced with other customized CF models (e.g., CACC, platooning) per application requirements. Further, this study uses the default HV behavior models obtained from the existing pure HV traffic, which may vary in emerging mixed traffic. For example, Zhao et al. (2020) showed that the behavior for an HV to follow a CAV may vary drastically from the existing HV CF behavior when the CAV has obvious features for the HV driver to identify, yet this behavior may remain unchanged if the HV cannot differentiate the vehicle type. In the cases that HV exhibit different driving behaviors, the new behavior models can be used instead of the default ones in this framework.

DOCUMENT OVERVIEW

Chapter 2 presents the mixed traffic simulation framework logic and its development. Chapter 3 describes the model calibration and validation using field experiments data. Chapter 4 introduces the basic guidance on the model implementation to which future uses can refer whiling implementing the mixed traffic simulation framework into existing simulators. Chapter 5 uses PTV Vissim as an example to implement the proposed model and conducts sensibility analyses on key parameters to test the impacts of the model on traffic performance. Chapter 6 concludes this study and gives possible future research directions.

CHAPTER 2. MODEL DEVELOPMENT AND LOGIC

DESCRIPTION OF MODEL LOGIC

This section briefly introduces the proposed mixed traffic simulation framework and the CAV LC model, as illustrated in Figure 1. The proposed framework can fully control HVs and CAVs in mixed traffic. A vehicle set $\mathcal{N}$ is defined containing N vehicles indexed by $n \in \mathcal{N}$: = {1, 2, …, $N\}$. Each vehicle is initialized with its type (i.e., HV or CAV) and route (i.e., origin and destination). CAV cooperation rate is also defined, indicating the probability of a CAV being cooperative to CAV LCs on an adjacent lane(s). For the HV control component, customized HV CF and LC strategies can be implemented according to the application requirements. Please refer to recent studies on HVs' responses to AVs with and without a differentiable appearance for HV behavior modeling in mixed traffic (Hamdar et al., 2019; Zhao et al., 2020). This study mainly focused on the CAV LC model, in boldface in Figure 1.

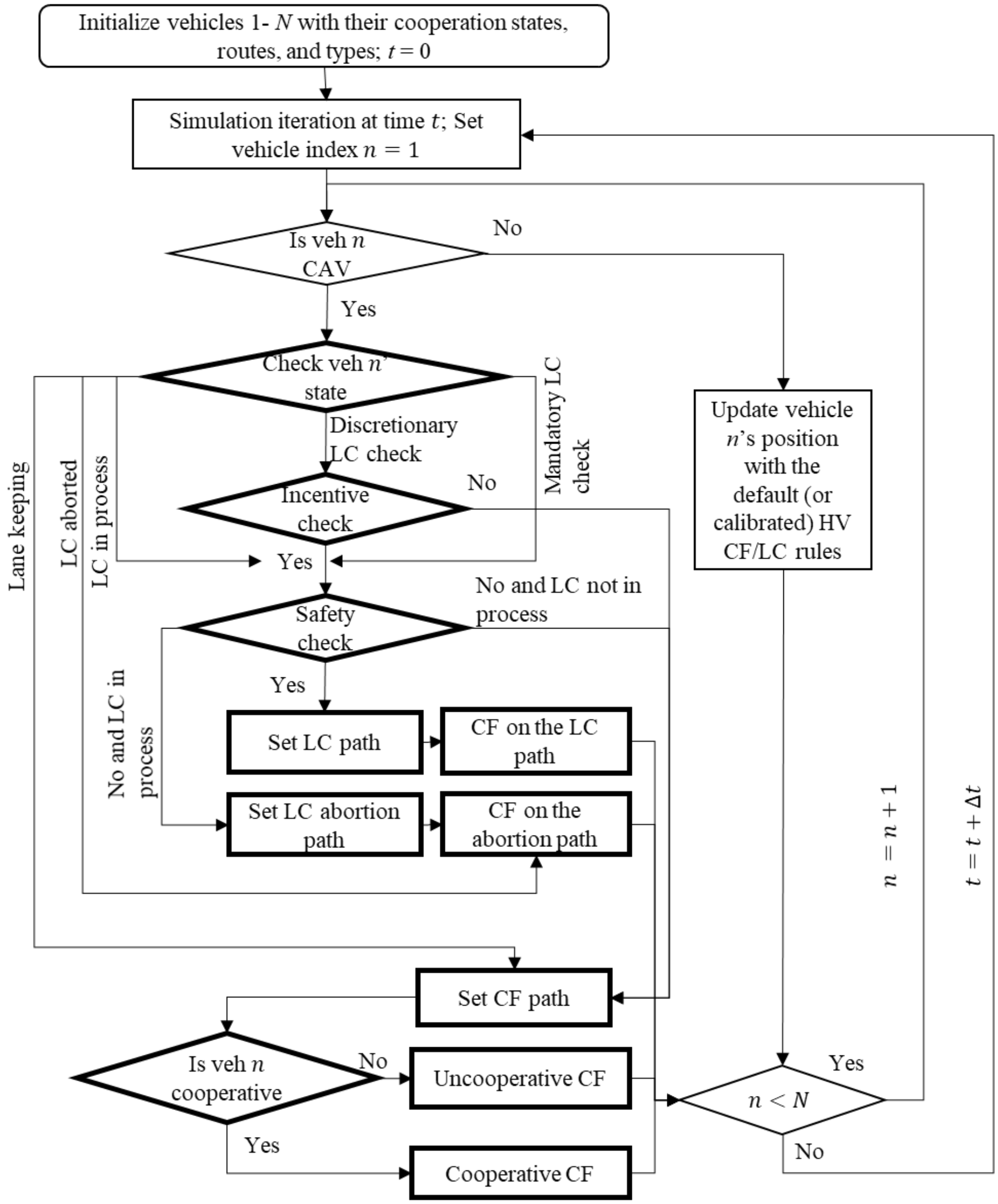

Source: FHWA.
Δt = simulation timestep.
CAV = connected and automated vehicle.
CF = car following.
HV = human-driven vehicle.
LC = lane changing.
N = total number of vehicles.
n = current object vehicle index.
t = current simulation time point.

Figure 1. Flowchart. The proposed mixed traffic simulation framework.

Connected and Automated Vehicle States

At simulation time *t*, CAV *n*'s possible states are listed as follows:

- Mandatory LC checking: CAV *n* changes to a specific lane to reach its destination. For example, CAVs "R" in the middle lane within the mandatory LC zone in Figure 2.
- Discretionary LC checking: CAV *n* can stay on any one of multiple lanes. For example, CAV "R" outside of the mandatory LC zone and CAVs "T" in Figure 2.
- Lane keeping: CAV *n* stays in the same lane to reach the destination or due to regulation (e.g., solid markings). For example, CAV "R" in the right lane within the mandatory LC zone.
- LC in process: CAV *n* has already initiated the LC movements. For example, the highlighted CAV "R" in the red solid circle in Figure 2.
- LC abortion in process: CAV *n* just aborted the LC to come back to the current lane. For example, the highlighted CAV "T" in the red dashed ellipse in Figure 2.

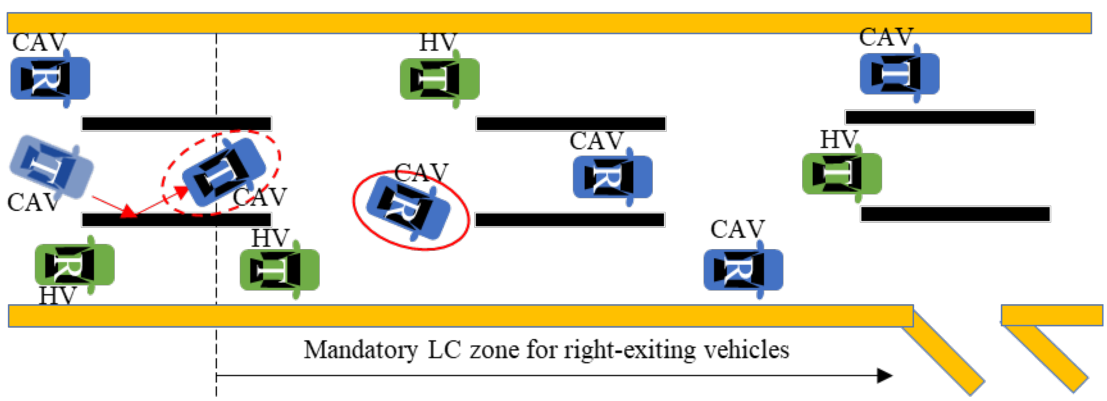

Source: FHWA.
CAV = connected and automated vehicle.
HV = human-driven vehicle.ss
LC = lane changing.
R = right-exiting vehicle.
T = through vehicle.

Figure 2. Illustration. Vehicle states.

Connected and Automated Vehicle States

As shown in Figure 3 the center line of the lane is set as CAV CF path (i.e., the red dashed line). At simulation time *t*, CAV *n*'s CF behavior is defined based on the cooperative state.

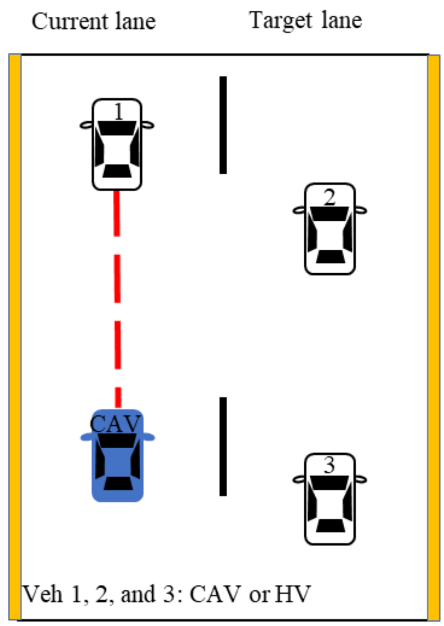

Source: FHWA.
CAV = connected and automated vehicle.
HV = human-driven vehicle.

Figure 3. Connected and automated vehicle car-following path.

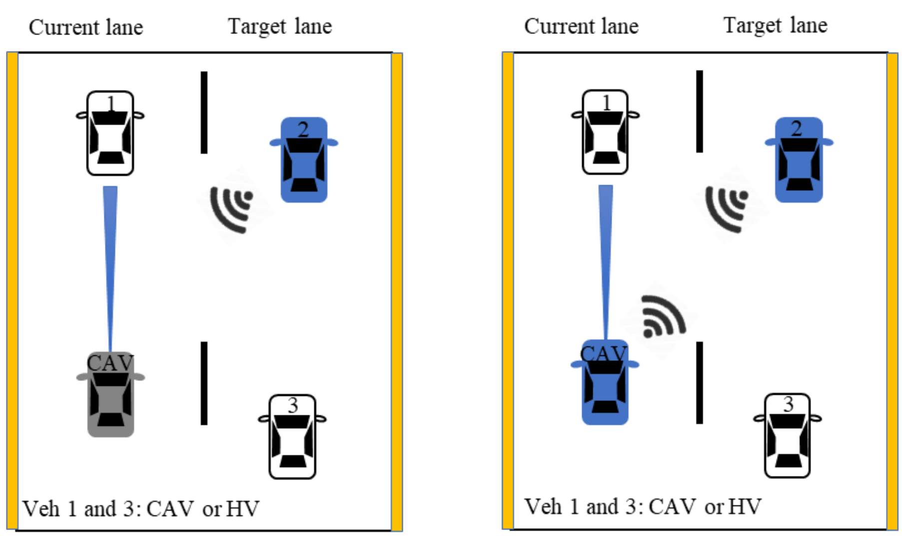

Source: FHWA.
CAV = connected and automated vehicle.
HV = human-driven vehicle.

(a) Uncooperative connected and automated vehicle.

(b) Cooperative connected and automated vehicle

Figure 4. Illustration. Uncooperative/cooperative connected and automated vehicle.

The CAV cooperative states are defined as follows:

- CAV *n* uncooperative: CAV *n* only follows the preceding vehicle in the current lane regardless of the LC signals(s) of the preceding CAV(s) in the neighboring lane(s), shown in Figure 4(a).
- CAV *n* cooperative: CAV *n* follows not only the preceding vehicle in the current lane but also the preceding CAV(s) in the neighboring lane(s) with the LC signal(s) on, shown in Figure 4(b).

Connected and Automated Vehicle Lane Changing

At simulation time *t*, CAV *n*'s LC behavior contains two components: LC decision-making and LC/LC abortion path generation and following.

Lane-Changing Decision-Making

LCs are divided into two categories: discretionary LCs and mandatory LCs. Discretionary LCs are optional and take place when vehicles want to make an LC to improve mobility (e.g., pass a slower-moving preceding vehicle). Mandatory LCs are implemented when vehicles make an LC to reach their desired destinations. The involved LC decision criteria are defined as follows:

- Lane marking criterion: Before any LC behavior, CAV *n* checks the current lane marking. The following criteria are checked only when the lane marking is dashed, communicating that LC behavior is permitted. Otherwise, CAV *n* is not allowed to make an LC now.

- Incentive criterion: Defined only for discretionary LCs. It asks whether CAV *n* can travel faster by conducting an LC to follow a vehicle in the target lane—i.e., vehicle 2 in Figure 5(a). If yes, the incentive criterion is met.

- Safety criterion: Defined for both discretionary LCs and mandatory LCs. It asks whether or not CAV *n*'s deceleration induced by following the preceding vehicle in the target lane—i.e., vehicle 2 in Figure 5(b)—is greater than a safety/comfort deceleration threshold and whether or not the deceleration of the following vehicle in the target lane—i.e., vehicle 3 in Figure 5(b)—induced by CAV *n*'s LC is greater than a safety/comfort deceleration threshold. If both are yes, the safety criterion is met.

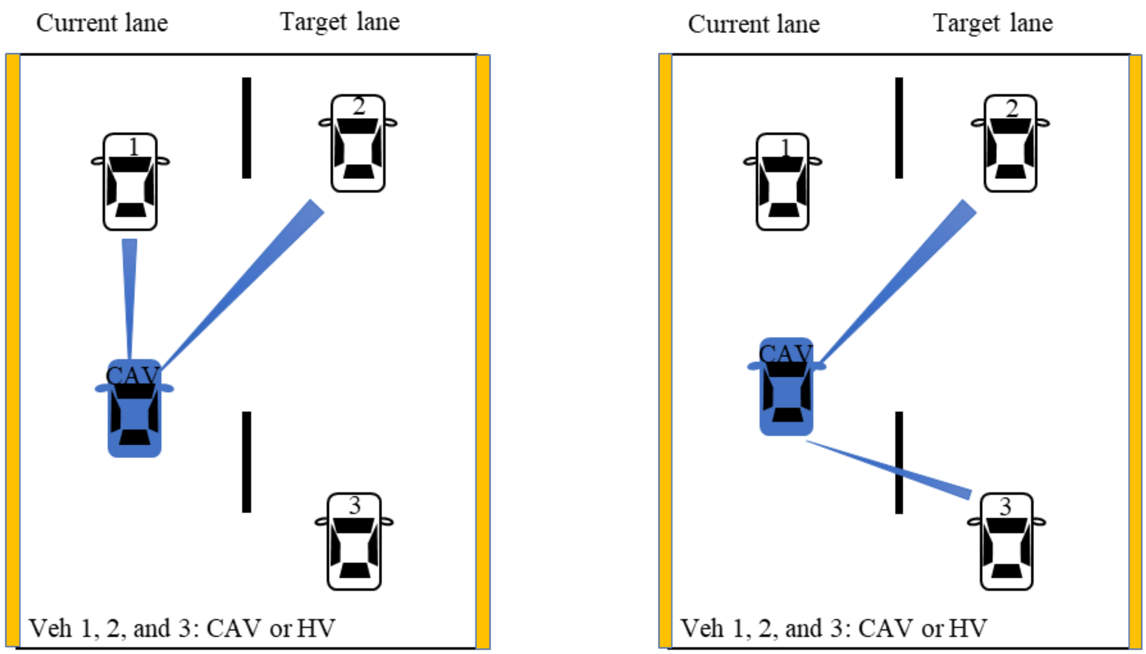

Source: FHWA.
CAV = connected and automated vehicle.
HV = human-driven vehicle.

(a) Incentive criterion. (b) Safety criterion.

Figure 5. Illustration. Incentive and safety criteria.

Lane Changing/Lane-Changing Abortion Path Generation and Following

For a discretionary LC, an LC path is generated and followed if both the incentive and safety criteria are met for CAV *n*. For a mandatory LC, an LC path is generated and followed if the safety criterion is met for CAV *n*. The safety criterion is continuously checked before the CAV crosses the lane marking. An LC abortion path is generated and followed if the safety criterion fails to be met before the CAV crosses the lane marking. This means CAV *n* goes back to its original lane to guarantee safety.

MODEL DEVELOPMENT

Connected and Automated Vehicle Car-Following Model

A linear ACC model (Milanés and Shladover 2014) is used to control CAVs longitudinal movements, formulated in Figure 6:

$$\tilde{a}_{\mathrm{CAV}}(t) = K_1\left(x_l(t) - x_{\mathrm{CAV}}(t) - C - v_{\mathrm{CAV}}(t)g_{\mathrm{CAV}}\right) + K_2\big(v_l(t) - v_{\mathrm{CAV}}(t)\big), \forall t \in \mathcal{T}$$

Figure 6. Equation. Linear adaptive cruise control model.

Where:

K_1 = parameter of the linear model with unit s^{-2}.

K_2 = parameter of the linear model with unit s^{-1}.
g_{CAV} = desired time gap of the CAV with unit s.
C = uniform vehicle length for CAVs and HVs with unit ft.
$x_{CAV}(t)$ = longitudinal position of the CAV at time t with unit ft.
$v_{CAV}(t)$ = speed of the CAV at time t with unit ft/s
$x_l(t)$ = longitudinal position of the preceding vehicle in the current lane at time t with unit ft.
$v_l(t)$ = speed of the preceding vehicle in the current lane at time t with unit ft/s.
$\tilde{a}_{CAV}(t)$ = target acceleration of the CAV at time t with unit ft/s^2.
s = second.
ft = foot.

Connected and Automated Vehicle Lane-Changing Model

Lane-Changing Decision-Making Model

First, the lane marking type between the current and target lanes is checked to verify whether or not the CAV is permitted to make an LC. According to the Manual of Uniform Traffic Control Devices (MUTCD 2006), dashed lane marking indicates drivers are permitted to make LCs; drivers are not permitted to change lanes when lane marking is solid. If the marking type is dashed, the marking criterion is met. Otherwise, the CAV maintains its current lane. Second, the incentive criterion checking is necessary for CAV discretionary LCs, formulated in Figure 7. The incentive criterion is only met when the target acceleration of the CAV following preceding vehicle in the target lane is greater than that in the current lane by a certain value, i.e., Δa plus a_{bias}.

$$\hat{a}_{\text{CAV}}(t) - \tilde{a}_{\text{CAV}}(t) > \Delta a + a_{bias}$$

Figure 7. Equation. Incentive criterion.

Where:
$\tilde{a}_{CAV}(t)$ = target acceleration of the CAV following preceding vehicle in the current lane at time t with unit ft/s^2.
$\hat{a}_{CAV}(t)$ = target acceleration of the CAV following preceding vehicle in the target lane at time t with unit ft/s^2.
Δa = LC threshold, preventing LCs when the associated advantage is marginal with unit ft/s^2.
a_{bias} = asymmetry term with a positive value for left turn and negative value for right turn with unit ft/s^2 (Treiber and Kesting, 2013), guaranteeing the keep-right directive rule.
s = second.
ft = foot.

Third, the safety criterion checking is necessary for both CAV discretionary and mandatory LCs. The safety criterion consists of two criteria with respect to the preceding and following vehicles in the target lane, respectively, as demonstrated in Figure 5(b).

First, the CAV checks the distance between the CAV longitudinal position and the preceding vehicle longitudinal position in the target lane when the LC is finished. $S(t)$ is the expected minimum safety distance calculated by Gipps' safe distance algorithm (Gipps, 1981), shown in Figure 8.

$$S(t) = v_{\mathrm{CAV}}(t)\tau_{\mathrm{CAV}} + \frac{\left(v_{\mathrm{CAV}}(t)\right)^2}{2b_{\mathrm{CAV}}} - \frac{\left(\hat{v}_l(t)\right)^2}{2\hat{b}_l}, \forall t \in \mathcal{T}$$

Figure 8. Equation. Gipps' safe distance.

Where:

τ_{CAV} = reaction time of the CAV with unit s.
b_{CAV} = maximum deceleration of the CAV with unit ft/s^2 (negative value).
$\hat{v}_l(t)$ = speed of the preceding vehicle in the target lane at time t with unit ft/s.
$\hat{b}_l$ = maximum deceleration of the preceding vehicle in the target lane at time t with unit ft/s^2 (negative value).
s = second.
ft = foot.

If $\hat{x}_l(t) - x_{\mathrm{CAV}}(t) - C \geqslant S(t)$, the CAV LC does not cause a deceleration to the CAV that is too dramatic (Wang et al., 2020). Hence, the safety criterion with respect to the preceding vehicle in the target lane is met. $\hat{x}_l(t)$ is the longitudinal position of the preceding vehicle at time t in the target lane with unit ft, $x_{\mathrm{CAV}}(t)$ is the longitudinal position of CAV n at time t with unit ft, and C is the uniform vehicle length for CAVs and HVs with unit ft.

The second criterion is for the following vehicle in the target lane, formulated in Figure 9. The intelligent driver model (IDM) is used to calculate the target acceleration of the following vehicle in the target lane $\hat{a}_f(t)$ (Treiber and Kesting, 2013; Wang et al., 2020).

$$\hat{a}_f(t) = \hat{w}_f\left[1 - \left(\frac{\hat{v}_f(t)}{v_{\mathrm{CAV}}(t)}\right)^{\delta} - \left(\frac{S^*(\hat{v}_f(t), \Delta v(t))}{\hat{S}(t)}\right)^2\right], \forall t \in \mathcal{T}$$

$$S^*(\hat{v}_f(t), \Delta v(t)) = s_0 + \max\left(0, \hat{v}_f(t)\Delta \mathrm{T} + \frac{\hat{v}_f(t)\left(v_{\mathrm{CAV}}(t) - \hat{v}_f(t)\right)}{2\sqrt{-\hat{w}_f\hat{b}_f}}\right), \forall t \in \mathcal{T}$$

$$\hat{S}(t) = x_{\mathrm{CAV}}(t) - \hat{x}_f(t) - C, \forall t \in \mathcal{T}$$

Figure 9. Equation. Target acceleration calculated by intelligent driver model.

Where:

s_0 = minimum gap with unit ft.
ΔT = time gap with unit s.
δ = acceleration exponent.
$\hat{w}_f$ = maximum acceleration of the following vehicle in the target lane at time t with unit ft/s^2.
$\hat{x}_f(t)$ = longitude position of the following vehicle in the target lane at time t with unit ft.
$x_{\mathrm{CAV}}(t)$ = longitude position of CAV n at time t with unit ft.
$\hat{v}_f(t)$ = speed of the following vehicle in the target lane at time t with unit ft/s.
$v_{\mathrm{CAV}}(t)$ = speed of CAV n at time t with unit ft/s.
$\Delta v(t) = v_{\mathrm{CAV}}(t) - \hat{v}_f(t)$ with unit ft/s.
$\hat{b}_f$ = maximum deceleration of the following vehicle in the target lane at time t with unit ft/s^2 (negative value).

C = uniform vehicle length for CAVs and HVs with unit ft.
s = second.
ft = foot.

If $\hat{a}_f(t) \geq \hat{b}_f(t)$, the CAV LC maneuver does not cause deceleration to the following vehicle in the target lane that is too dramatic. Hence, the safety criterion concerning the following vehicle in the target lane is met.

Lane Changing/Lane-Changing Abortion Path Generation and Following Model

After all criteria are met, a smooth two-dimensional (2D) spatial LC path is generated and updated at each timestep for the CAV to follow and complete the LC reaching its final target position, obtained with the equation in Figure 10, safely and comfortably. A sine-function-based LC path (i.e., the black dotted curve in Figure 12) is applied to generate a smooth trajectory at time t composed of discrete points (x'_{CAV}, y'_{CAV}) in the local coordinate system, formulated in Figure 10 (Wang et al., 2020):

$$y'_{\mathrm{CAV}}(t) = \frac{R^{\mathrm{Y}}(t)}{2\pi}[\Delta\mathrm{X} - \sin(\Delta\mathrm{X})] + y_{\mathrm{CAV}}(t), x'_{\mathrm{CAV}} \in [x_{\mathrm{CAV}}(t), x_2(t) - S(t) - C], \forall t \in \mathcal{T}$$

$$\Delta\mathrm{X} = \frac{2\pi}{R^{\mathrm{X}}(t)}\left(x'_{\mathrm{CAV}}(t) - x_{\mathrm{CAV}}(t)\right)$$

$$R^{\mathrm{X}}(t) = x_2(t) - S(t) - x_{\mathrm{CAV}}(t) - C, \forall t \in \mathcal{T}$$

$$R^{\mathrm{Y}}(t) = y_{\mathrm{CAV}}(t) - y_2(t), \forall t \in \mathcal{T}$$

Figure 10. Equation. A sin-function-based lane-changing path.

Where:
$x_{\mathrm{CAV}}(t)$, $y_{\mathrm{CAV}}(t)$ = longitudinal and lateral positions of the CAV at time t with unit ft.
$x_2(t)$, $y_2(t)$ = longitudinal and lateral positions of vehicle 2 in Figure 12 at time t with unit ft.
$S(t)$ = safety distance calculated in Figure 8.
C = uniform vehicle length for CAVs and HVs with unit ft.
$R^{\mathrm{X}}(t)$, $R^{\mathrm{Y}}(t)$ = longitudinal gap and the lateral offset between the CAV and vehicle 2 at time t with unit ft.
s = second.
ft = foot.

In the large-scale simulation, a linear function LC path (i.e., the red solid line in Figure 12) was used to replace the sine-function-based LC path (i.e., the black dotted curve in Figure 12) for simplicity, formulated in Figure 11:

$$y'_{\mathrm{CAV}}(t) = y_{\mathrm{CAV}}(t) + \frac{R^{\mathrm{Y}}(t)}{R^{X}(t)}\left(x'_{\mathrm{CAV}}(t) - x_{\mathrm{CAV}}(t)\right), x'_{\mathrm{CAV}} \in [x_{\mathrm{CAV}}(t), x_2(t) - S(t) - C], \forall t \in \mathcal{T}$$

Figure 11. Equation. A linear function lane-changing path.

The safety criterion is continuously checked before the CAV crosses the lane marking. The CAV LC is aborted if the safety criterion fails to be met. In this scenario, the LC abortion path (i.e., the green dashed line in Figure 12) is generated and followed. The CAV goes back to its original lane following the LC abortion path. With the LC abortion mechanism, CAV LC safety can be guaranteed.

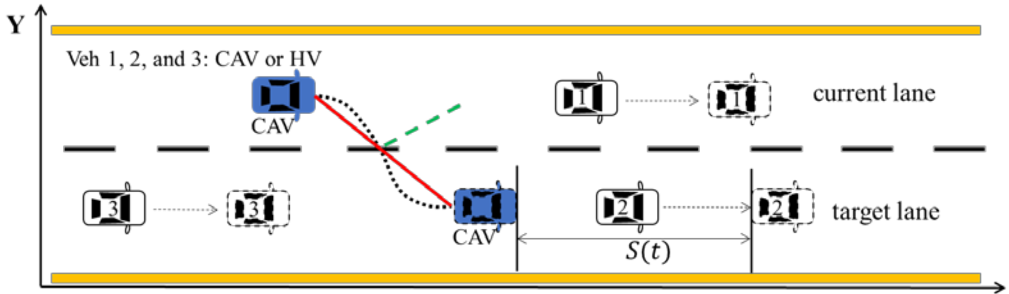

Source: FHWA.
CAV = connected and automated vehicle.
HV = human-driven vehicle.
S(t) = expected minimum safety distance.

Figure 12. Illustration. Connected and automated vehicle lane changing/lane-changing abortion path.

During the LC process, the CAV uses the ACC model to follow the preceding vehicles in the current and target lanes—i.e., vehicles 1 and 2 in Figure 13(a)—before it passes the lane marking. After the CAV passes the lane marking, it only follows the current preceding vehicle—i.e., vehicle 2 in Figure 13(b)—using the ACC model.

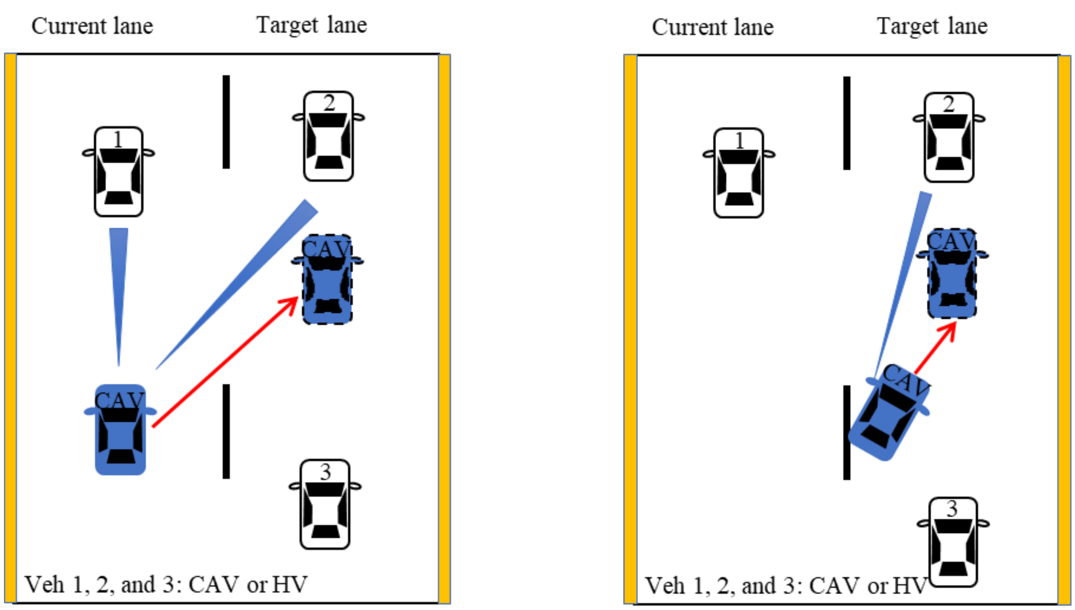

Source: FHWA.
CAV = connected and automated vehicle.
HV = human-driven vehicle.

(a) Car following before the lane marking. (b) Car following after the lane marking.

Figure 13. Illustration. Car following of lane changing.

During the LC abortion process, the CAV uses the ACC model to follow the preceding vehicles in the current lane (i.e., vehicle 1 in Figure 14) and goes back to the center line of the lane.

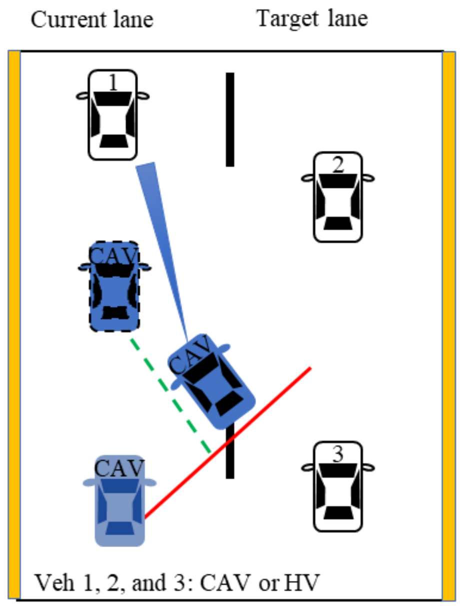

Source: FHWA.
CAV = connected and automated vehicle.
HV = human-driven vehicle.

Figure 14. Illustration. Car following of lane-changing abortion.

CHAPTER 3. MODEL CALIBRATION AND VALIDATION

MODEL CALIBRATION

To demonstrate how to calibrate the proposed CAV LC model, the researchers used field data collected from small-scale field experiments of a CAV mandatory LC model with three surrounding HVs collected during a previous study (Wang et al., 2020). The CAV mandatory LC model flow chart is presented in Figure 15. This chart is just a simplification of the proposed CAV LC model in the mandatory LC context in Figure 1. In the field experiments, the CAV used the ACC model to follow HVs 1 and 2, and continuously checked the safety criterion considering HV 2 and HV 3. Once the safety criterion was met, a sine-function-based LC path (i.e., Figure 12) was generated for the CAV to follow. The safety criterion was continuously checked in the LC path following process, and the LC maneuver was aborted if the safety criterion failed to be met before the CAV crossed the lane marking. When the CAV reached the target position, i.e., the center line of the target lane, it successfully made an automated LC.

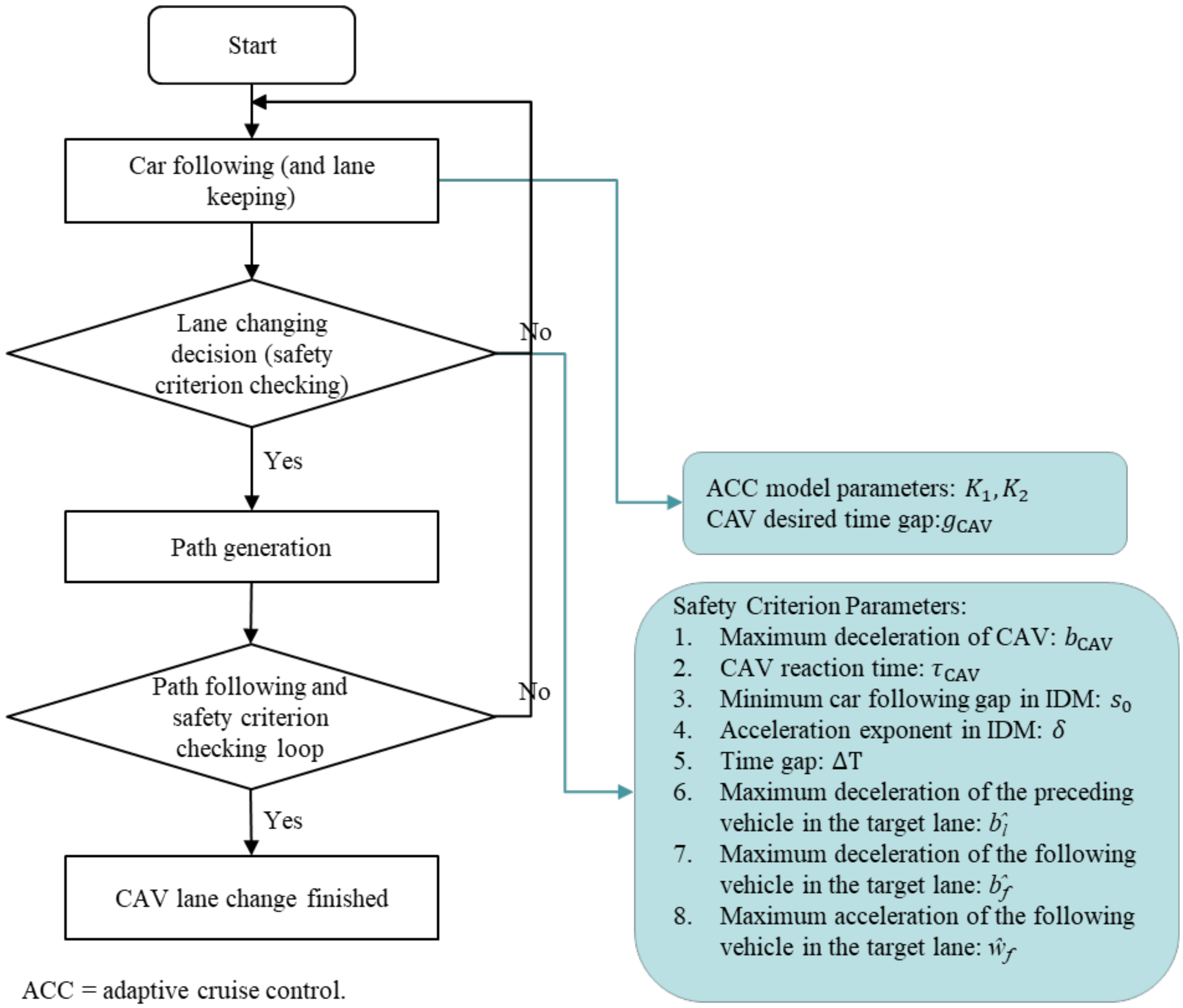

ACC = adaptive cruise control.
CAV = connected and automated vehicle.
HV = human-driven vehicle.
IDM = intelligent driver model.
Source: FHWA.

Figure 15. Flowchart. Connected and automated vehicle mandatory lane-changing logic with key parameters.

The test track segment for the small-scale field experiment was a straight, two-lane road with length (L) of 0.5 mi and lane width (D) of 11.5 feet. All vehicles' lengths (C) were 15 feet. The sine-function-based LC path was implemented during the field experiments.

Four cases (c ∈ {1, 2, 3, 4}) of experiments representing four different traffic situations were conducted.

- In the first case (c = 1), the preceding vehicle in the current lane (i.e., HV 1 in Figure 12) was asked to decelerate, creating a shock wave. The preceding vehicle in the target lane (i.e., HV 2 in Figure 12) kept a relatively constant speed and the following vehicle in the target lane (i.e., HV 3 in Figure 12) was not aggressive, yielding to the CAV LC.

- In the second case (c = 2), HV 2 was asked to decelerate, creating a shock wave. HV 1 kept relatively constant speed and HV 3 was not aggressive, yielding to the CAV LC.
- In the third case (c = 3), HVs 1 and 2 in Figure 12 both kept relatively constant speed and HV 3 was not aggressive, yielding to the CAV LC.
- In the final case (c = 4), HVs 1 and 2 in Figure 12 both kept relatively constant speed, but HV 3 was accelerating instead of yielding to the CAV LC, which represented aggressive driving; this forced the CAV to abort the LC maneuver.

The speeds of HV 1 and HV 2 were kept within 9–41 ft/s during the experiments (Wang et al., 2020). Note that two runs of the experiments with the same settings were conducted for each case. The data from the first run of four cases were used for simulation model calibration; the second run data were used for simulation model validation. Small-scale simulation with the same setting as the field experiments was conducted to calibrate the CAV mandatory LC model parameters (listed in Figure 15), a component of the mixed traffic simulation model. HVs 1, 2, and 3 trajectories were controlled to replicate the field experiment trajectories and the CAV trajectory was generated using the proposed CAV LC model. RMSE of the CAV longitudinal positions was formulated as shown in Figure 16:

$$RMSE_c^x(\beta) = \sqrt{\frac{1}{Q_c}\sum_{q=1}^{Q_c}\left(x_{c,q}^{obs} - x_{c,q}^{cal}(\beta)\right)^2}$$

Figure 16. Equation. Root mean square error of the connected and automated vehicle longitudinal positions in model calibration.

Where:

$x_{c,q}^{obs}$, $x_{c,q}^{cal}$ = field-observed and calibrated longitudinal positions of the CAV at time point q in case c with unit ft.

Q_c = total number of time points in case c.

β = parameters set.

ft = foot.

The error between the calibrated LC time point and field-observed LC time point was formulated as shown in Figure 17:

$$E_c^t(\beta) = |t_c^{LCobs} - t_c^{LCcal}(\beta)|$$

Figure 17. Equation. The error between the calibrated lane-changing time point and field-observed lane-changing time point in model calibration.

Where:

t_c^{LCobs}, t_c^{LCcal} = field-observed and calibrated LC time points in case c with unit s.

β = parameters set.

s = second.

Thus, the calibration optimization objective was formulated as shown in Figure 18:

$$\min_{\beta} \frac{1}{4} \sum_{c=1}^{4} \left(RMSE_c^x(\beta) + E_c^t(\beta) \right)$$

Figure 18. Equation. The calibration optimization objective.

Where:

$RMSE_c^x$ = root mean square error of the CAV longitudinal positions in case c.
E_c^t = error between the calibrated LC time point and field-observed LC time point in case c.
β = parameters set.

RMSE of the CAV speeds was also calculated to measure the calibration results, formulated as shown in Figure 19:

$$RMSE_c^v(\beta) = \sqrt{\frac{1}{Q_c} \sum_{q=1}^{Q_c} \left(v_{c,q}^{obs} - v_{c,q}^{cal}(\beta) \right)^2}$$

Figure 19. Equation. Root mean square error of the connected and automated vehicle speeds in model calibration.

Where:

$v_{c,q}^{obs}$, $v_{c,q}^{cal}$ = field-observed and calibrated speeds of the CAV at time point q in case c with unit ft/s.
Q_c = total number of time points in case c.
β = parameters set.
ft/s = foot per second.

The interior-point method was used to find the optimal parameter values. As shown in Figure 20, the objective function value was stable at 6.19 after iteration 7 with an average $RMSE_c^x(\beta)$ of 4.79 ft and an average $E_c^t(\beta)$ of 1.4 s, indicating a good calibration result (shown in Table 1). The parameters β calibration results are provided in Table 2. The detailed CAV longitudinal positions, speeds, and LC time calibration results of four cases are provided in Figure 21, Figure 22, Figure 23, and Figure 24. The calibrated CAV trajectories (i.e., the dashed curves) were almost consistent with the field-observed trajectories (i.e., the solid curves) with minor differences with an average $RMSE_c^x(\beta)$ value of 4.79 ft and an average $E_c^t(\beta)$ value of 1.18 ft/s. The difference between the calibrated and field-observed LC time point was less than 3 s across all cases.

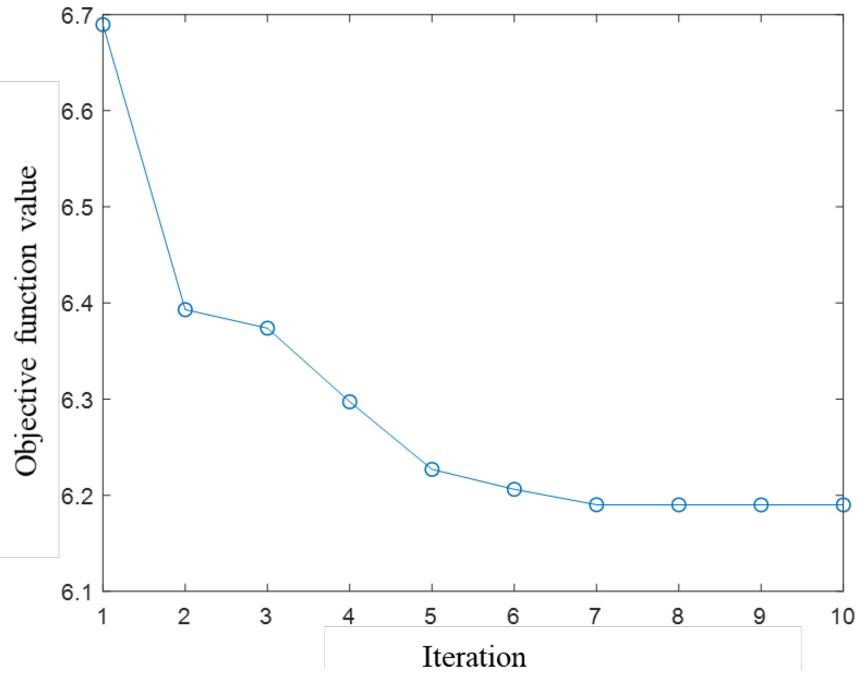

Source: FHWA.

Figure 20. Graph. Calibration objective function convergence.

Table 1. Calibration results summary.

Case	t_c^{LCobs} (s)	t_c^{LCcal} (s)	E_c^t (s)	$RMSE_c^x$ (ft)	$RMSE_c^v$ (ft/s)
$c = 1$	36.2	39.0	2.8	6.10	1.80
$c = 2$	11.5	13.4	1.9	3.48	1.28
$c = 3$	30.2	31.1	0.9	3.02	0.66
$c = 4$	inf	inf	0.0	6.53	0.98
Average	\	\	1.4	4.79	1.18

inf = no lane-changing behavior. ft = foot. ft/s = foot per second. *RMSE* = root mean square error. s = second. t_c^{LCobs} = field-observed lane-changing time point in case *c*. t_c^{LCcal} = calibrated lane-changing time point in case *c*. E_c^t = error between the calibrated lane-changing time point and field-observed lane-changing time point. $RMSE_c^x$ = root mean square error of the connected and automated vehicle calibrated longitudinal positions. $RMSE_c^v$ = root mean square error of the connected and automated vehicle calibrated speeds. \ = not applicable.

Table 2. Parameters calibration results.

Parameters $\boldsymbol{\beta}$	Calibration Results
$K_1(s^{-2})$	0.1997
$K_2(s^{-1})$	0.6820
$g_{\mathrm{CAV}}(s)$	1.5265
$b_{\mathrm{CAV}}(ft/s^2)$	-14.7600
$\tau_{\mathrm{CAV}}(s)$	0.9000
$s_0(ft)$	13.1324
δ	2.0000
$\Delta T(s)$	1.3000
$\hat{b}_l$ / $\hat{b}_f(ft/s^2)$	-13.7795
$\hat{w}_f(ft/s^2)$	13.1234

b_{CAV} = CAV maximum deceleration rate. $\hat{b}_l$ = maximum deceleration of the preceding vehicle in the target lane. $\hat{b}_f$ = maximum deceleration of the following vehicle in the target lane. ft = foot. ft/s^2 = foot per second squared. g_{CAV} = CAV desired time gap. K_1, K_2 = adaptive cruise control model parameter. s = second. s_0 = minimum car-following gap in intelligent driver model. $\hat{w}_f$ = maximum acceleration of the following vehicle in the target lane. ΔT = time gap in intelligent driver model. δ = acceleration exponent in intelligent driver model. τ_{CAV} = CAV reaction time.

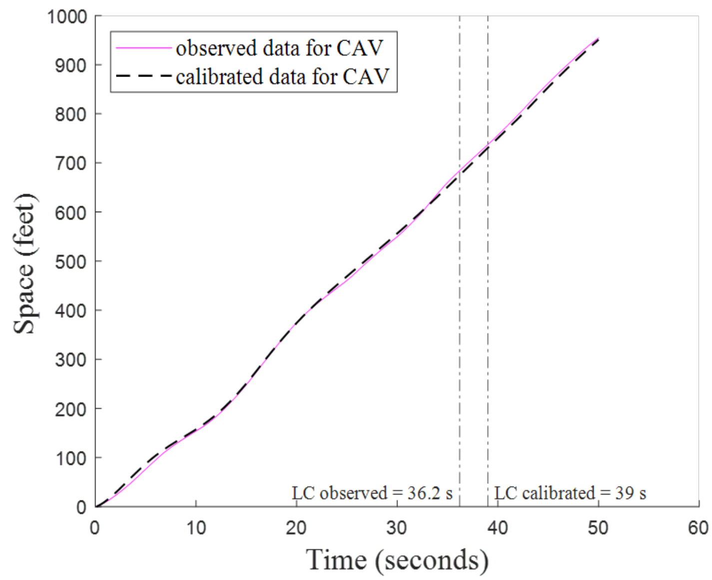

Source: FHWA.
CAV = connected and automated vehicle.
LC = lane changing.

(a) Vehicle trajectories in case 1.

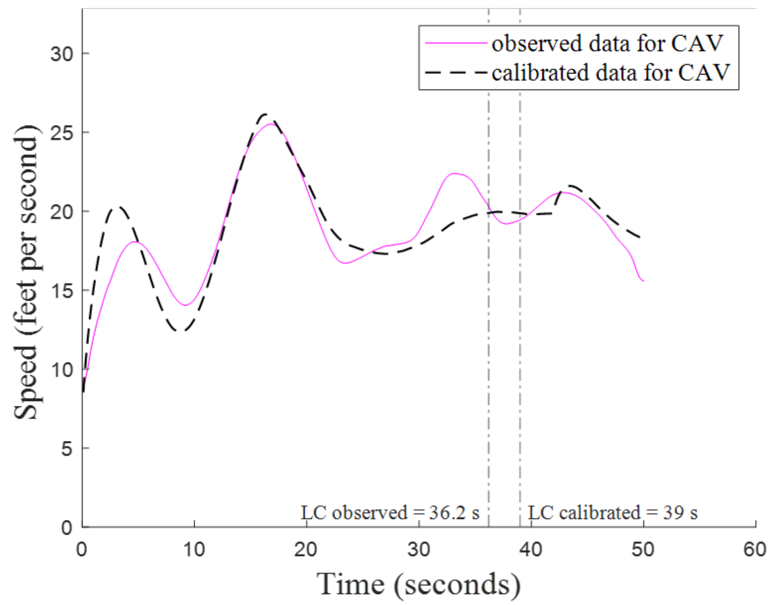

Source: FHWA.
CAV = connected and automated vehicle.
LC = lane changing.

(b) Vehicle speeds in case 1.

Figure 21. Graph. Calibration results of case 1.

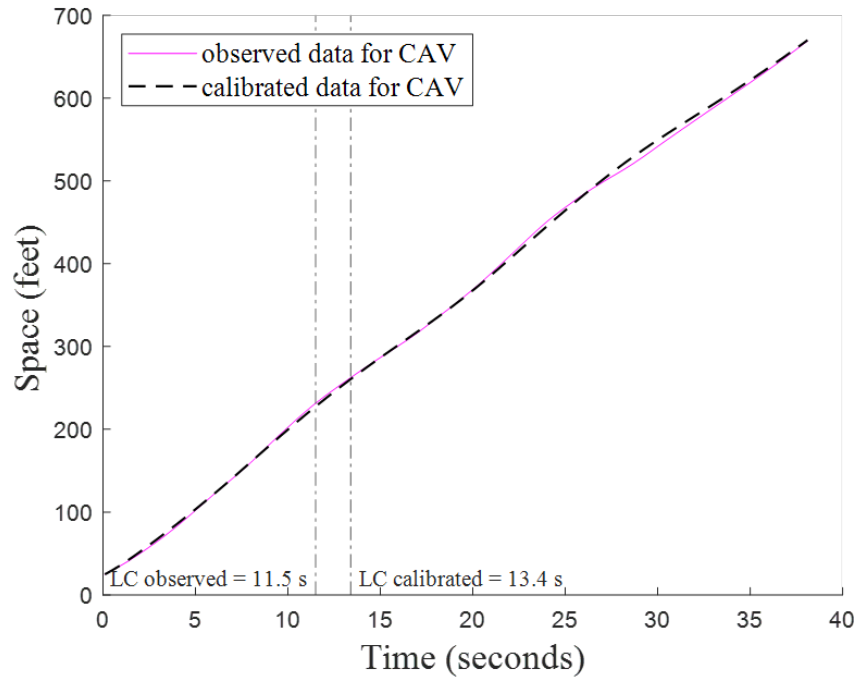

Source: FHWA.
CAV = connected and automated vehicle.
LC = lane changing.

(a) Vehicle trajectories in case 2.

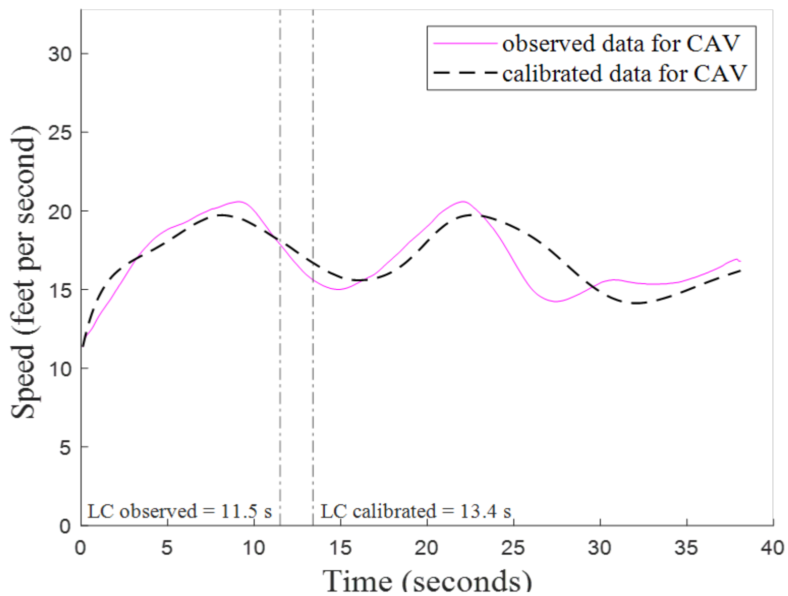

Source: FHWA.
CAV = connected and automated vehicle.
LC = lane changing.

(b) Vehicle speeds in case 2.

Figure 22. Graph. Calibration results of case 2.

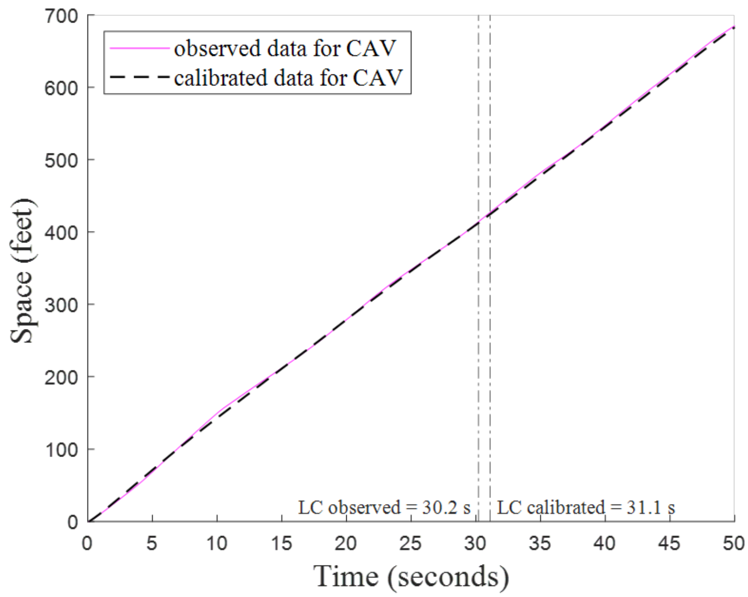

Source: FHWA.
CAV = connected and automated vehicle.
LC = lane changing.

(a) Vehicle trajectories in case 3.

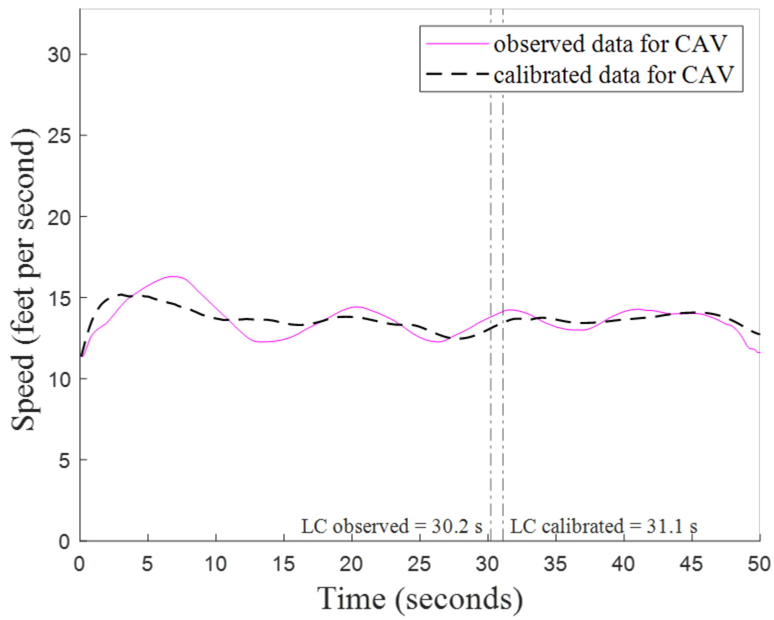

Source: FHWA.
CAV = connected and automated vehicle.
LC = lane changing.

(b) Vehicle speeds in case 3.

Figure 23. Graph. Calibration results of case 3.

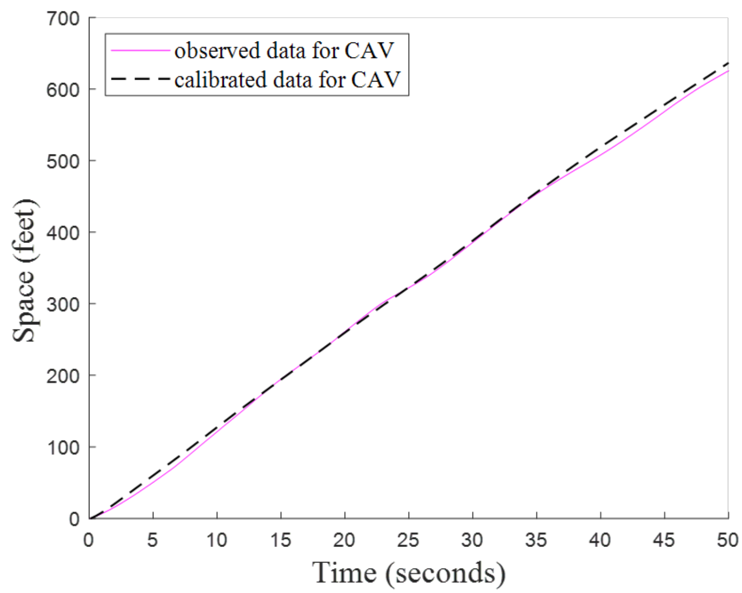

Source: FHWA.
CAV = connected and automated vehicle.

(a) Vehicle trajectories in case 4.

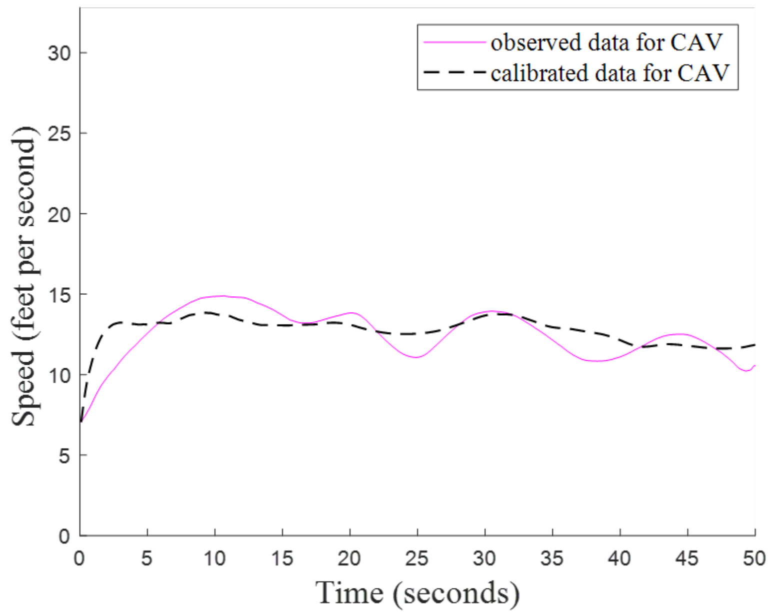

Source: FHWA.
CAV = connected and automated vehicle.

(b) Vehicle speeds in case 4.

Figure 24. Graph. Calibration results of case 4.

MODEL VALIDATION

The second run data of the four cases were used for model validation. RMSE of CAV longitudinal positions $RMSE_c^x$ and speeds $RMSE_c^v$ were calculated as shown in Figure 25 for four cases using the calibrated parameters from the first run.

$$RMSE_c^x(\beta) = \sqrt{\frac{1}{Q_c}\sum_{q=1}^{Q_c}\left(x_{c,q}^{obs} - x_{c,q}^{val}(\beta)\right)^2}$$

$$RMSE_c^v(\beta) = \sqrt{\frac{1}{Q_c}\sum_{q=1}^{Q_c}\left(v_{c,q}^{obs} - v_{c,q}^{val}(\beta)\right)^2}$$

Figure 25. Equation. Root mean square errors of the connected and automated vehicle longitudinal positions and speeds in model validation.

Where:

$x_{c,q}^{obs}$, $x_{c,q}^{val}$ = field-observed and validated longitudinal positions of the CAV at time point q in case c with unit ft.

$v_{c,q}^{obs}$, $v_{c,q}^{val}$ = field-observed and validated speeds of the CAV at time point q in case c with unit ft/s.

Q_c = total number of time points in case c.

β = parameters set.

The validation results are summarized in Table 3. The error between the validated LC time and field observed LC time was only 0.53 s on average. $RMSE_c^x$ had an average value of 6.89 ft. Compared with the calibration results (i.e., the LC time error with an average value of 1.4 s and $RMSE_c^x$ with an average value of 4.79 ft), the validation results showed less difference, which suggested a valid calibration. Detailed validation results are provided in Figure 26, Figure 27, Figure 28, and Figure 29.

Table 3. Validation results summary.

Case	t_c^{LCobs} (s)	t_c^{LCval} (s)	E_c^t (s)	$RMSE_c^x$ (ft)	$RMSE_c^v$ (ft/s)
$c = 1$	53.6	53.8	0.2	5.09	0.82
$c = 2$	26.0	26.2	0.6	6.14	1.44
$c = 3$	21.3	22.6	1.3	6.14	1.05
$c = 4$	inf	inf	0.0	10.24	1.25
Average	\	\	0.53	6.89	1.15

inf = no lane-changing behavior. ft = foot. ft/s = foot per second. *RMSE* = root mean square error. s = second. t_c^{LCobs} = field-observed lane-changing time point in case *c*. t_c^{LCval} = validated lane-changing time point in case *c*. E_c^t = error between the validated lane-changing time point and field-observed lane-changing time point. $RMSE_c^x$ = root mean square error of the connected and automated vehicle validated longitudinal positions. $RMSE_c^v$ = root mean square error of the connected and automated vehicle validated speeds. \ = not applicable.

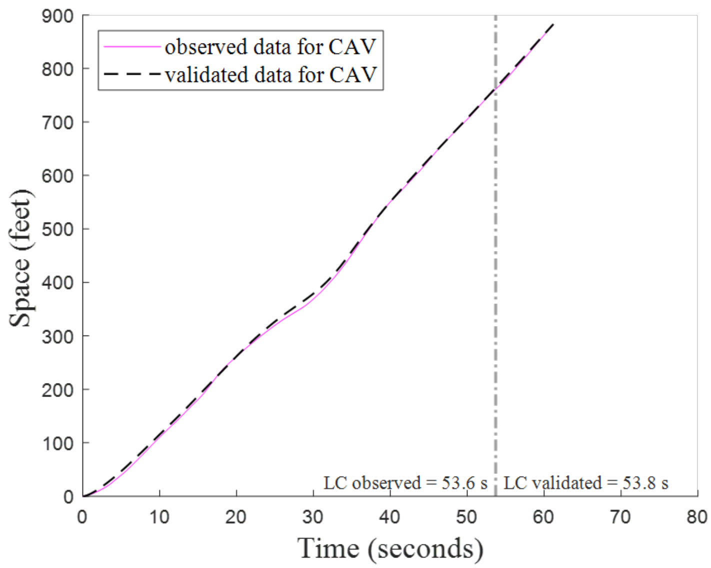

Source: FHWA.
CAV = connected and automated vehicle.
LC = lane changing.

(a) Vehicle trajectories in case 1.

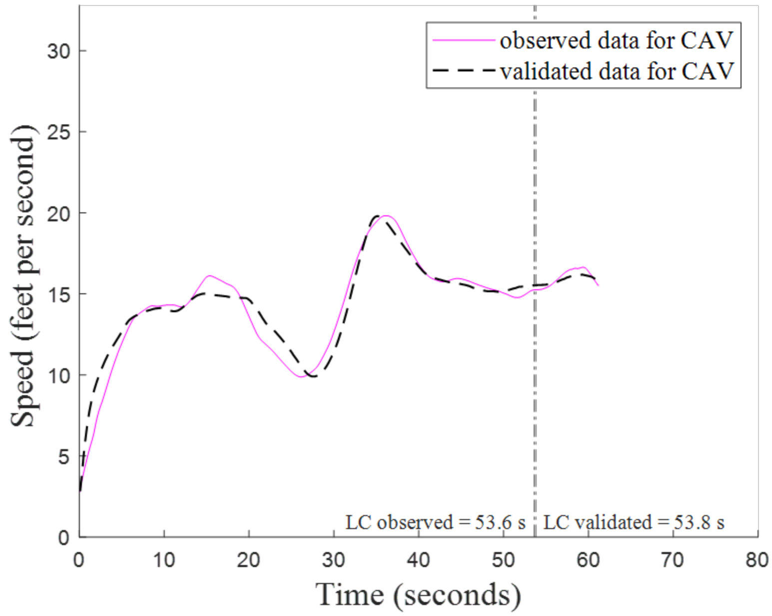

Source: FHWA.
CAV = connected and automated vehicle.
LC = lane changing.

(b) Vehicle speeds in case 1.

Figure 26. Graph. Validation results of case 1.

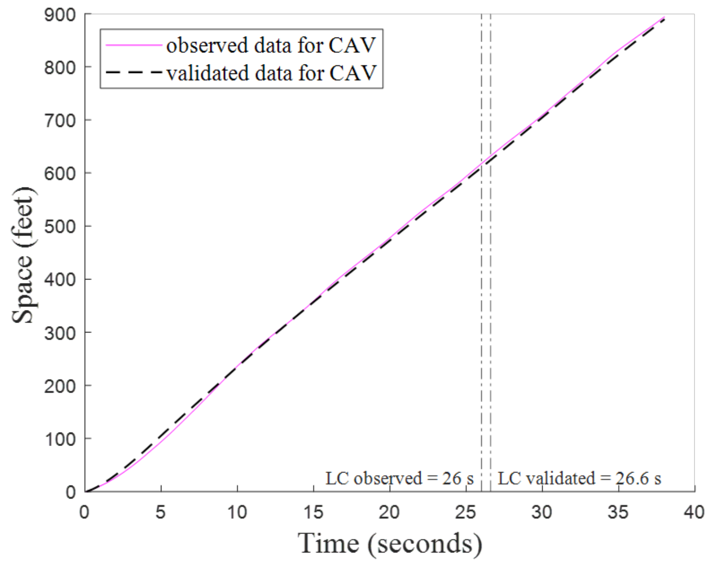

Source: FHWA.
CAV = connected and automated vehicle.
LC = lane changing.

(a) Vehicle trajectories in case 2.

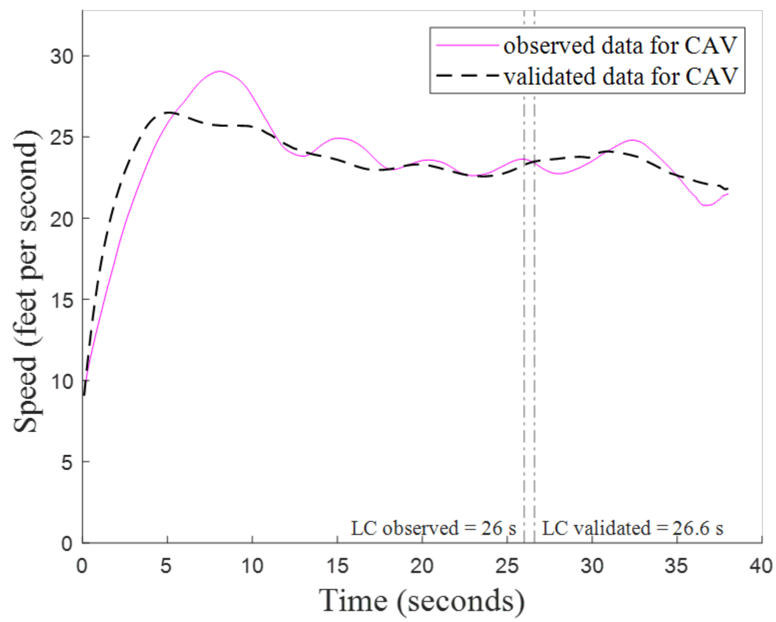

Source: FHWA.
CAV = connected and automated vehicle.
LC = lane changing.

(b) Vehicle speeds in case 2.

Figure 27. Graph. Validation results of case 2.

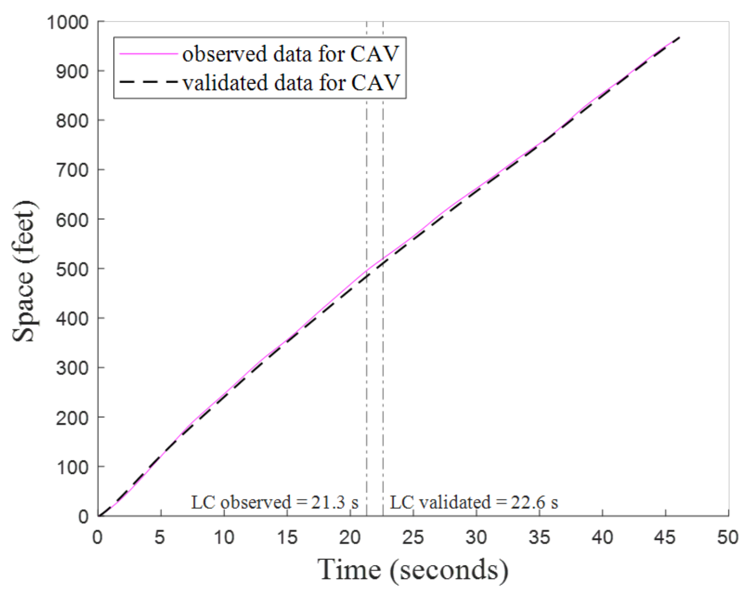

Source: FHWA.
CAV = connected and automated vehicle.
LC = lane changing.

(a) Vehicle trajectories in case 3.

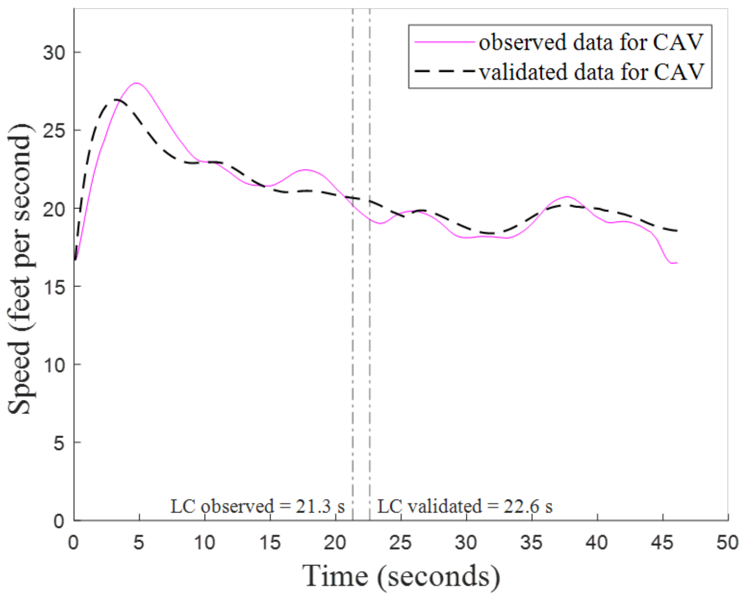

Source: FHWA.
CAV = connected and automated vehicle.
LC = lane changing.

(b) Vehicle speeds in case 3.

Figure 28. Graph. Validation results of case 3.

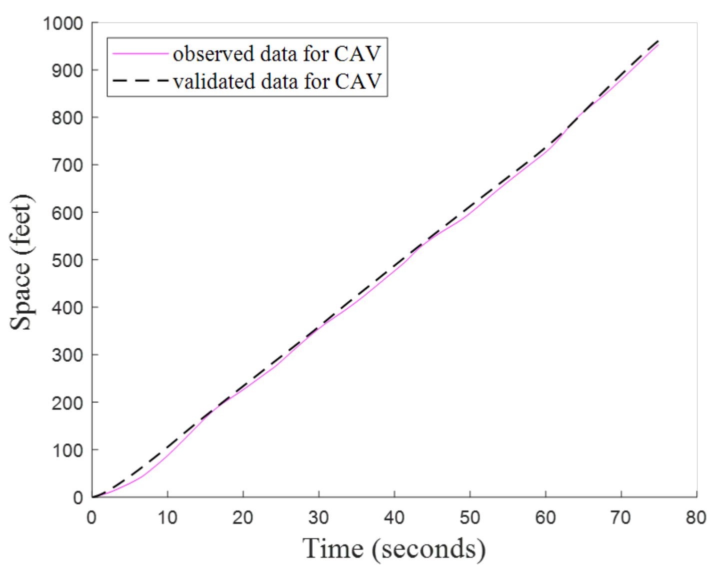

Source: FHWA.
CAV = connected and automated vehicle.

(a) Vehicle trajectories in case 4.

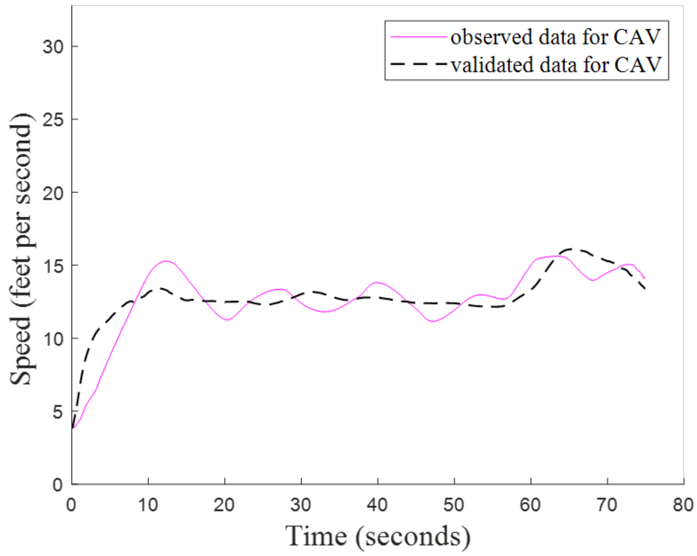

Source: FHWA.
CAV = connected and automated vehicle.

(b) Vehicle speeds in case 4.

Figure 29. Graph. Validation results of case 4.

CHAPTER 4. BASIC INFORMATION ON MODEL IMPLEMENTATION

The following steps are important to implement the proposed model into existing microsimulation platforms:

- Create a customized roadway network according to the application requirements.
- Set roadway throughput, assign vehicle types (e.g., HV, CAV) when populating them, define CAV cooperation rate, initialize CAV and HV routes (i.e., origins and destinations), and define desired speeds in the demand loading module.
- Replace the simulator's default vehicle CF and LC rules with the proposed CAV CF and LC rules for CAV control in the vehicle dynamic module.

Note that the simulator's default vehicle control rules can still be used for HV control. Figure 30 provides an illustration. There is a three-lane main road, a single-lane on-ramp, and a single-lane off-ramp. The traffic stream moves from left to right with mainline throughput q_1 and on-ramp throughput q_2. CAV penetration rates r_1^{CAV} and r_2^{CAV}, CAV diverging rates (i.e., right-exiting rates) r_1^{CAVdiv} and r_2^{CAVdiv}, and HV diverging rates r_1^{HVdiv} and r_2^{HVdiv} are defined for mainline and on-ramp, respectively. CAV cooperative rate is defined as φ, denoting the probability of a CAV being cooperative. Vehicles are randomly generated based on these predefined parameters.

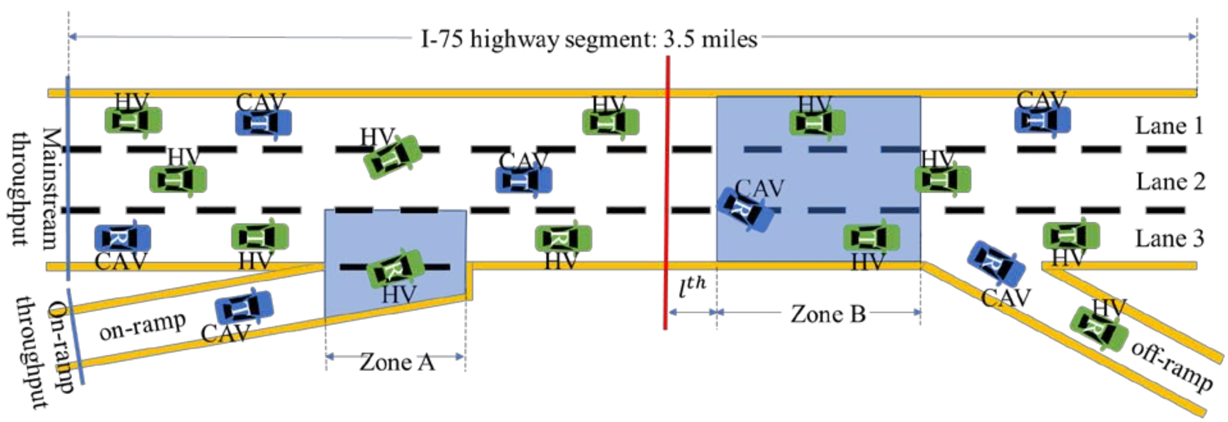

Source: FHWA.
CAV = connected and automated vehicle.
HV = human-driven vehicle.
l^{th} = throughput measurement location.
R = right-exiting vehicle.
T = through vehicle.

Figure 30. Illustration. The mixed traffic simulation framework implementation.

Two mandatory LC zones (i.e., zone A and zone B), shaded in Figure 30, were defined for this illustration segment because of the requirements of on-ramp merging and off-ramp diverging. Zone A with a length of L_A defined the mandatory LC area where on-ramp CAVs had to merge into the main lanes. Zone B with a length of L_B defined the mandatory LC area that right-exiting CAVs had to reach the right-most lane to exit the freeway through the off-ramp. The other areas were the CAV discretionary LC area. Note that existence of the mandatory LC zones would vary per geometric scenario. If there is no on-ramp, zone A does not exist. If there is no off-ramp, zone B does not exist. If there is no ramp at all, neither zone exists.

CHAPTER 5. USE CASE AND SENSITIVITY STUDY

To illustrate how to apply the entire simulation framework (including the proposed CAV LC model and the HV model in a mixed traffic environment), this section presents a large-scale case study with a commercial traffic simulator. Note that emerging CAV technology has experienced and will experience rapid change and diversification from the prototypes to commercial vehicles. The associated parameter settings in the LC model may change and diversify over the developments. Since these changes cannot be observed or accurately predicted, it is important to conduct sensitivity analyses to show how different values of the key parameters impact the traffic performance.

IMPLEMENTATION OF THE DEVELOPED MODEL INTO A TRAFFIC SIMULATION TOOL

PTV Vissim was used to implement the mixed traffic simulation framework on the I–75 highway segment, located in Tampa, Florida, as shown in Figure 31. The program was coded in C++ programming language in Microsoft® Visual Studio® integrated development environment (Microsoft Visual Studio 2019) to generate the external DriverModel.DLL, which was used for CAV control in the microsimulation software. The calibration parameters (see Table 2) were used in the simulation.

- The selected roadway segment created in the microsimulation software was about 3.27 mi with three main lanes, a single-lane on-ramp, and a single-lane off-ramp, shown in Figure 31. Zone A and Zone B were set as 0.19 mi and 0.87 mi in length, respectively.

- In the congested traffic simulation default case, mainline and on-ramp throughputs q_1 and q_2 were set as 4,500 vehicles per hour (vehicle/h) and 1,200 vehicle/h. In the uncongested traffic simulation default case, mainline and on-ramp throughputs q_1 and q_2 were set as 3,000 vehicle/h and 1,200 vehicles/h. All other parameters were identical for both default cases. CAV diverging rates r_1^{CAVdiv} and r_2^{CAVdiv} were set as 20 percent for the mainline and on-ramp traffic, HV diverging rates r_1^{HVdiv} and r_2^{HVdiv} were set as 20 percent for the mainline and on-ramp traffic, CAV penetration rates r_1^{CAV} and r_2^{CAV} were set as 50 percent for the mainline and on-ramp traffic, CAV cooperation rate φ was set as 50 percent, and incentive criterion threshold Δa and bias a_{bias} were set as 0.3 ft/s^2 and 0.9 ft/s^2, respectively. Vehicles were randomly generated based on these parameters, with their desired speeds around 100 ft/s in the mainline and 80 ft/s in the on-ramp. The simulation duration was set as 5 minutes in default with 0.1 s as the timestep.

- CAVs were controlled through an external DriverModel.dll that implements the proposed model and HVs were controlled using the simulator default CF/LC rules (PTV Group, 2018).

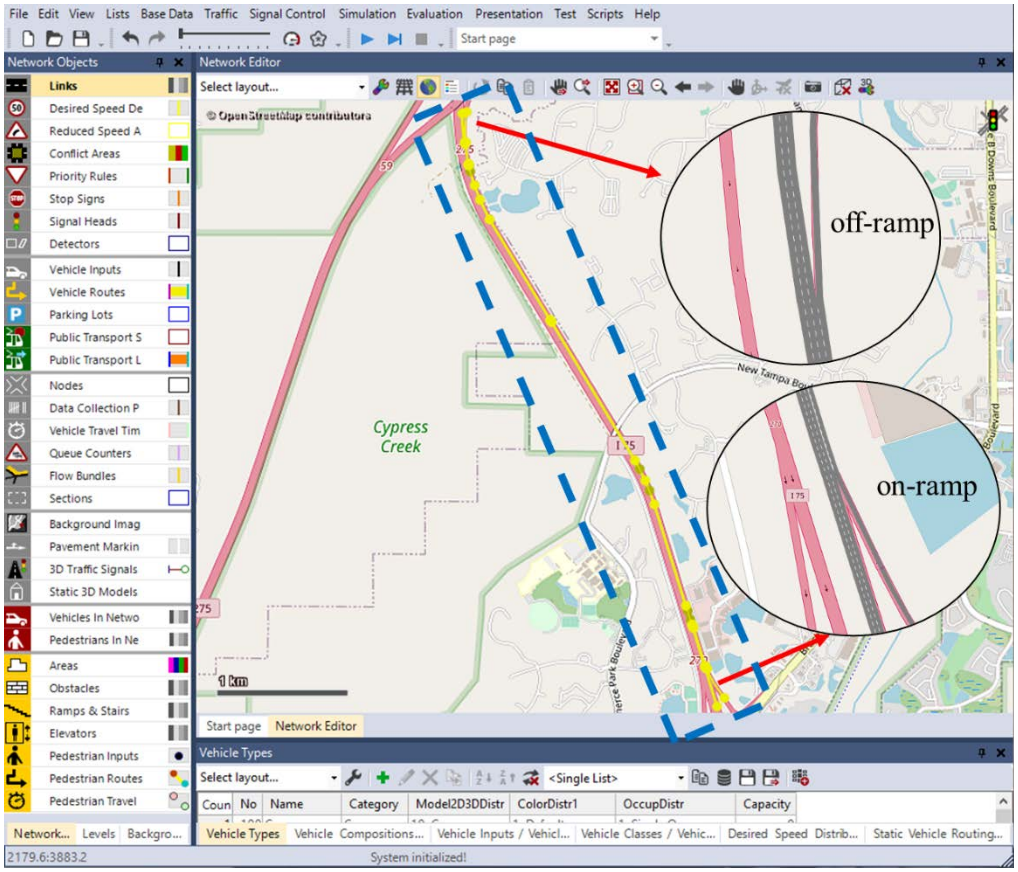

Created with PTV Vissim. Source: FHWA.

Figure 31. Screenshot. Study road segment.

DESIGN OF SIMULATION EXPERIMENTS

To investigate the impacts of CAV LC maneuvers on traffic system performance, sensitivity analyses were conducted on key parameters r_1^{CAV}, r_2^{CAV}, φ, Δa, and a_{bias} with one of the key parameters changed and other parameters kept the same. Vehicle average speed and speed standard deviation along the study roadway segment were used to measure traffic mobility and stability performance, respectively.

Vehicle set $\mathcal{N}$ was separated into CAV set $j \in \mathcal{J} := \{1, 2, \ldots, J\}$ and HV set $k \in \mathcal{K} := \{1, 2, \ldots, K\}$. The CAV average speed $\bar{v}_{\text{CAV}}$ in the simulation period was formulated as shown in Figure 32:

$$\bar{v}_{\text{CAV}} = \frac{\sum_{j=1}^{j=J} \frac{\sum_{t=0}^{t=T_j} v_j(t)}{T_j}}{J}$$

Figure 32. Equation. The connected and automated vehicle average speed.

Where:

T_j = number of time points that CAV j was running during a simulation period.
$v_j(t)$ = CAV j speed at time point t with unit ft/s.

J = total number of CAVs.
ft/s = foot per second.

The CAV speed standard deviation $\mathrm{STD}v_{\mathrm{CAV}}$ in the simulation period was formulated as shown in Figure 33

$$\mathrm{STD}_{v_{\mathrm{CAV}}} = \frac{\sum_{j=1}^{j=J} \sqrt{\frac{\sum_{t=0}^{t=T_j} (v_j(t) - \hat{v}_j)^2}{T_j}}}{J}$$

Figure 33. Equation. The connected and automated vehicle speed standard deviation.

Where:
T_j = number of time points that CAV j was running during a simulation period.
$v_j(t)$ = CAV j speed at time point t with unit ft/s.
$\hat{v}_j$ = average speed of CAV j in the simulation period with unit ft/s.
J = total number of CAVs.
ft/s = foot per second.

The HV average speed $\bar{v}_{\mathrm{HV}}$ in the simulation period was formulated as shown in

$$\bar{v}_{\mathrm{HV}} = \frac{\sum_{k=1}^{k=K} \frac{\sum_{t=0}^{t=T_k} v_k(t)}{T_k}}{K}$$

Figure 34:

$$\bar{v}_{\mathrm{HV}} = \frac{\sum_{k=1}^{k=K} \frac{\sum_{t=0}^{t=T_k} v_k(t)}{T_k}}{K}$$

Figure 34. Equation. The human-driven vehicle average speed.

Where:
T_k = number of time points that HV k was running during a simulation period.
$v_k(t)$ = HV k speed at time point t with unit ft/s.
K = total number of HVs.
ft/s = foot per second.

The HV speed standard deviation $\mathrm{STD}v_{\mathrm{HV}}$ in the simulation period was formulated as shown in Figure 35:

$$\mathrm{STD}_{v_{\mathrm{HV}}} = \frac{\sum_{k=1}^{k=K} \sqrt{\frac{\sum_{t=0}^{t=T_k} (v_k(t) - \hat{v}_k)^2}{T_k}}}{K}$$

Figure 35. Equation. The human-driven vehicle speed standard deviation.

Where:

T_k = number of time points that HV k was running during a simulation period.
$v_k(t)$ = HV k speed at time point t with unit ft/s.
$\hat{v}_k$ = average speed of HV k in the simulation period with unit ft/s.
K = total number of HVs.
ft/s = foot per second.

The average speed across all vehicles $\bar{v}_{\text{all}}$ in the simulation period is formulated as shown in

$$\bar{v}_{\text{all}} = \frac{\sum_{j=1}^{j=J} \frac{\sum_{t=0}^{t=T_j} v_j(t)}{T_j} + \sum_{k=1}^{k=K} \frac{\sum_{t=0}^{t=T_k} v_k(t)}{T_k}}{J+K}$$

Figure 36:

$$\bar{v}_{\text{all}} = \frac{\sum_{j=1}^{j=J} \frac{\sum_{t=0}^{t=T_j} v_j(t)}{T_j} + \sum_{k=1}^{k=K} \frac{\sum_{t=0}^{t=T_k} v_k(t)}{T_k}}{J+K}$$

Figure 36. Equation. The average speed across all vehicles.

Where:

T_j = number of time points that CAV j was running during a simulation period.
$v_j(t)$ = CAV j speed at time point t with unit ft/s.
T_k = number of time points that HV k was running during a simulation period.
$v_k(t)$ = HV k speed at time point t with unit ft/s.
J = total number of CAVs.
K = total number of HVs.

The speed standard deviation across all vehicles $\text{STD}v_{\text{all}}$ in the simulation period was formulated

$$\text{STD}_{v_{\text{all}}} = \frac{\sum_{j=1}^{j=J} \sqrt{\frac{\sum_{t=0}^{t=T_j} (v_j(t) - \hat{v}_j)^2}{T_j}} + \sum_{k=1}^{k=K} \sqrt{\frac{\sum_{t=0}^{t=T_k} (v_k(t) - \hat{v}_k)^2}{T_k}}}{J+K}$$

as shown in Figure 37:

$$\text{STD}_{v_{\text{all}}} = \frac{\sum_{j=1}^{j=J} \sqrt{\frac{\sum_{t=0}^{t=T_j} (v_j(t) - \hat{v}_j)^2}{T_j}} + \sum_{k=1}^{k=K} \sqrt{\frac{\sum_{t=0}^{t=T_k} (v_k(t) - \hat{v}_k)^2}{T_k}}}{J+K}$$

Figure 37. Equation. The speed standard deviation across all vehicles.

Where:

T_j = number of time points that CAV j was running during a simulation period.
$v_j(t)$ = CAV j speed at time point t with unit ft/s.
$\hat{v}_j$ = average speed of CAV j in the simulation period with unit ft/s.
J = total number of CAVs.
T_k = number of time points that HV k was running during a simulation period.
$v_k(t)$ = HV k speed at time point t with unit ft/s.
$\hat{v}_k$ = average speed of HV k in the simulation period with unit ft/s.
K = total number of HVs.
ft/s = foot per second.

CAV, HV, and total traffic throughput (q_{CAV}, q_{HV}, and q_{all}) during a 5-minute simulation period were also measured at the location where the red line is located in Figure 30, and l^{th} is set as 1,640 ft. Note that researchers assumed $r_1^{CAV} = r_2^{CAV} = r^{CAV}$ in the simulation, indicating that CAV penetration rates were the same in the mainline and on-ramp traffic.

SIMULATION RESULTS

This section presents the simulation results. A CAV discretionary LC process is demonstrated in Figure 38. Sensitivity analyses results of congested traffic simulation are provided in Figure 39, Figure 40, Figure 41, and Figure 42. Sensitivity analyses results of uncongested traffic simulation are provided in Figure 43, Figure 44, Figure 45, and Figure 46. These results provide insight into understanding mixed traffic and provide basic suggestions for engineering practice.

Lane-Changing Process Demonstration

In Figure 38(a), the CAV met both the incentive criterion and the safety criterion with respect to vehicles 2 and 3; thus, the CAV initiated the discretionary LC. In Figure 38(b), the CAV was crossing the lane marking. By Figure 38(c), the CAV finished the discretionary LC, as it had arrived at the center line of the target lane. The mandatory LC process is not presented because it is a similar movement, albeit under different circumstances.

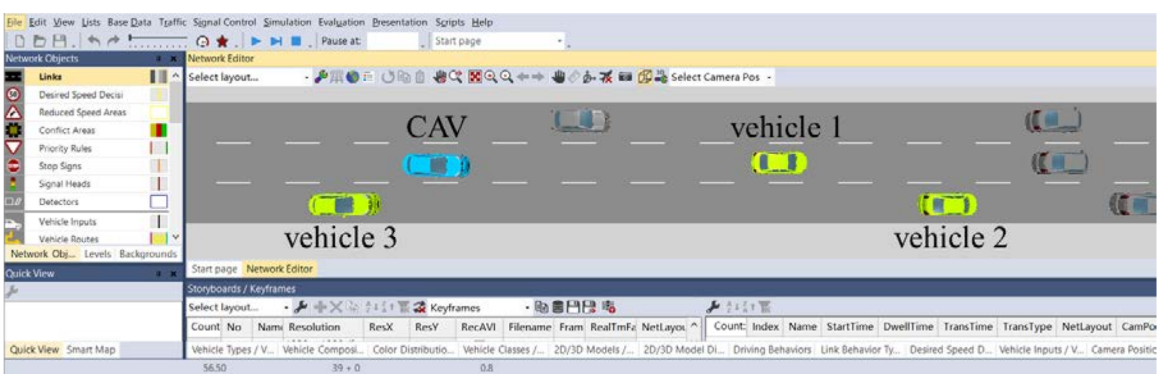

Created with PTV Vissim. Source: FHWA.
CAV = connected and automated vehicle.

(a) Discretionary lane-changing initiated.

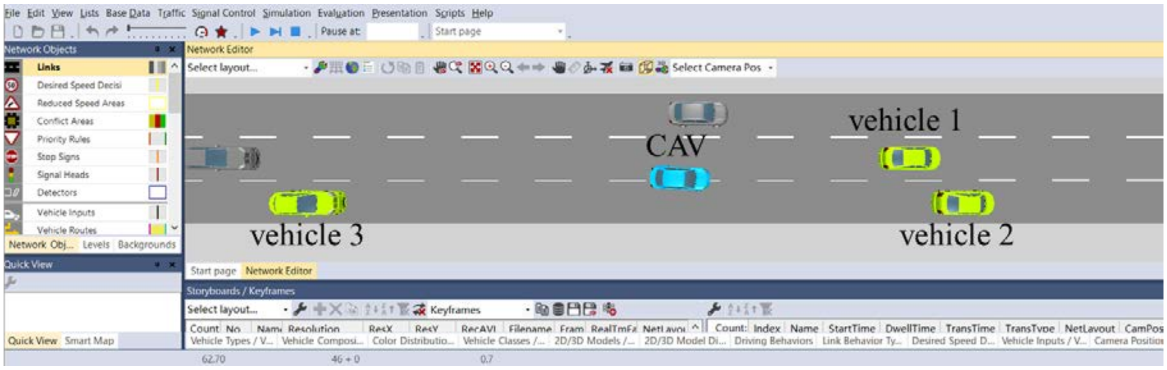

Created with PTV Vissim. Source: FHWA.
CAV = connected and automated vehicle.

(b) Discretionary lane-changing in process.

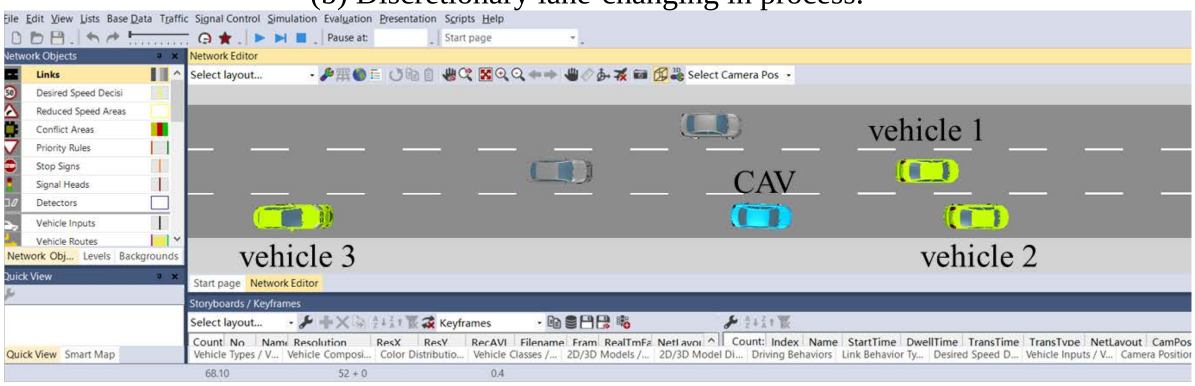

Created with PTV Vissim. Source: FHWA.
CAV = connected and automated vehicle.

(c) Discretionary lane-changing finished.

Figure 38. Screenshots. Connected and automated vehicle lane-changing process.

Sensitivity Analysis Results of Congested Traffic

The researchers used average speed as a surrogate for mobility performance: the greater the average speed, the better the mobility. The speed standard deviation was used to measure stability performance: the greater the speed standard deviation, the worse the stability. Vehicle throughput was another measurement of mobility performance.

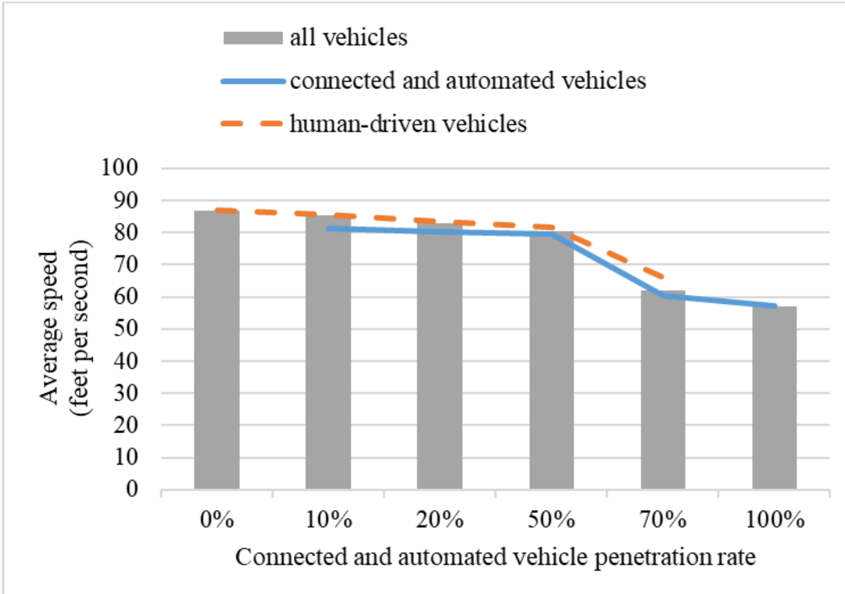

Source: FHWA.
% = percent.

(a) Average speed versus connected and automated vehicle penetration rate.

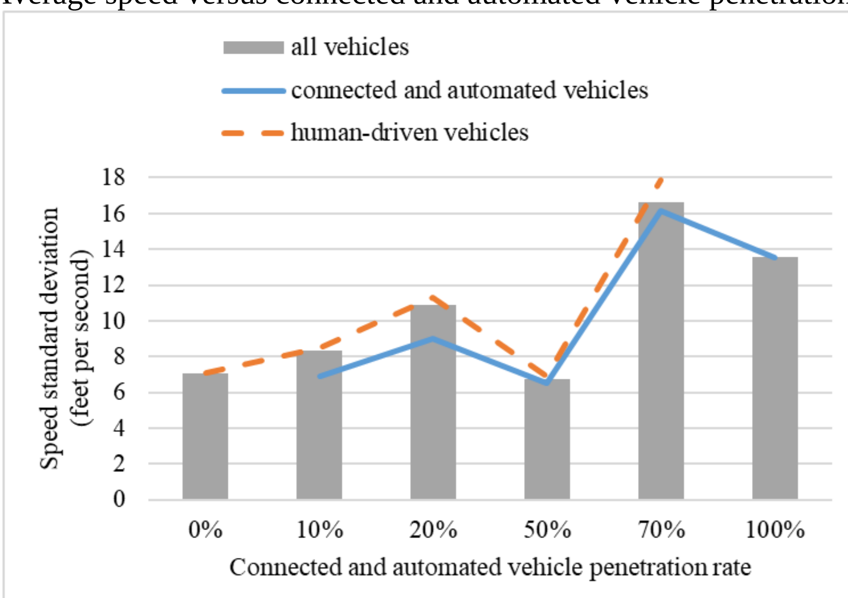

Source: FHWA.
% = percent.

(b) Speed standard deviation versus connected and automated vehicle penetration rate.

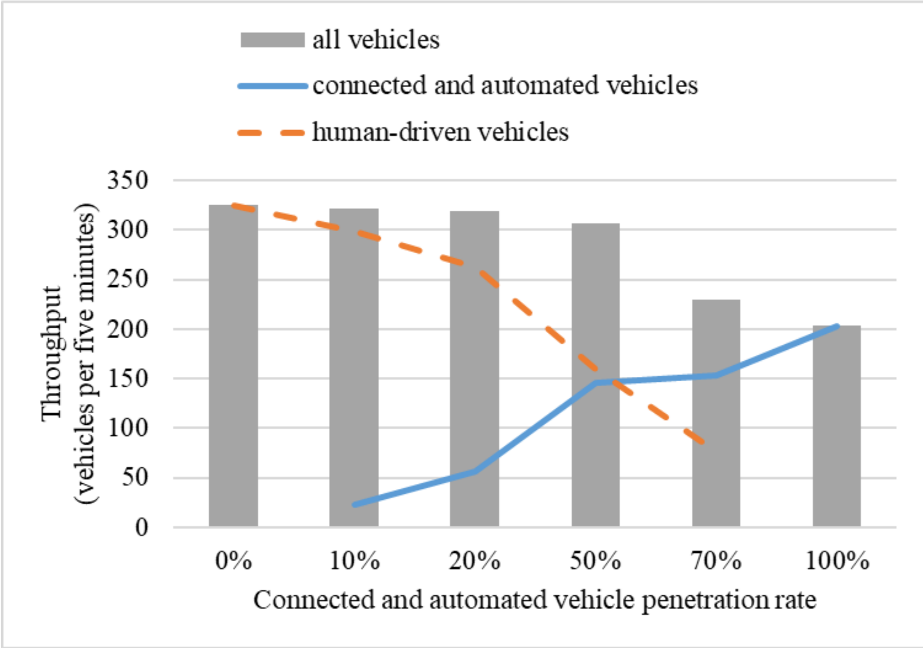

Source: FHWA.
% = percent.

(c) Throughput versus connected and automated vehicle penetration rate.

Figure 39. Graph. Sensitivity analysis on connected and automated vehicle penetration rate under congested traffic.

The results in Figure 39 showed that as the CAV penetration rate r^{CAV} increased, mobility performance degraded. This is primarily because the CAV CF and LC models used here were calibrated with data from a lab vehicle with more conservative driving rules than an average human driver for safety concerns (see the previous section for related calibration and verification). As a result, CAVs produced a longer average headway than HVs. Thus, as the CAV penetration rate increased, the average headway increased in the mixed traffic and thus the mobility measures degraded. These results are not completely out of context since CAV technologies are expected to have conservative settings in the initial deployment stage for safety concerns as well.

As r^{CAV} increased, the stability performance fluctuated. Increases in r^{CAV} resulted in more CAV LCs that caused more traffic oscillation and led to worse stability performance. Yet, as r^{CAV} kept increasing, probably because more cooperative CAVs would be present and their cooperation behavior improved the stability performance. Note that the best stability performance was observed when r^{CAV} = 50 percent. If the calibrated CAV model had a shorter time headway, it is expected that both the mobility and stability performance would have improved with increasing r^{CAV}, which yet asks for verifications in future studies.

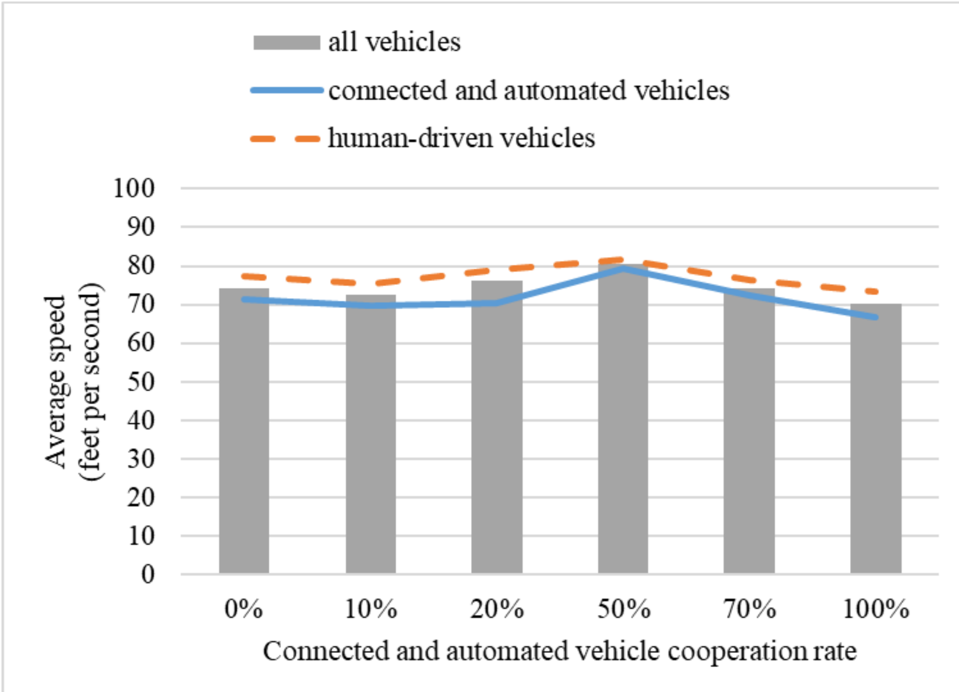

Source: FHWA.
% = percent.

(a) Average speed versus connected and automated vehicle cooperation rate.

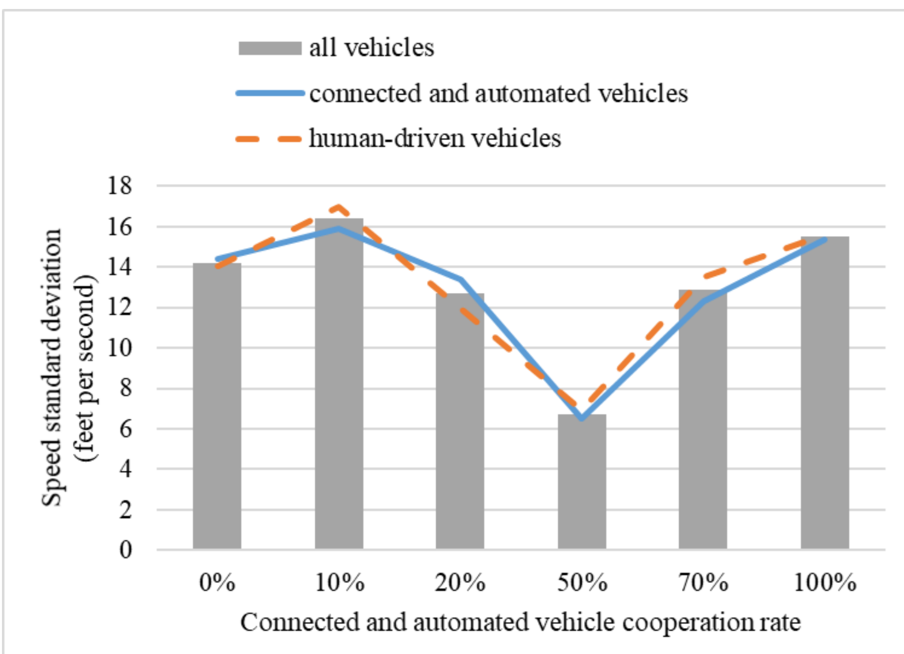

Source: FHWA.
% = percent.

(b) Speed standard deviation versus connected and automated vehicle cooperation rate.

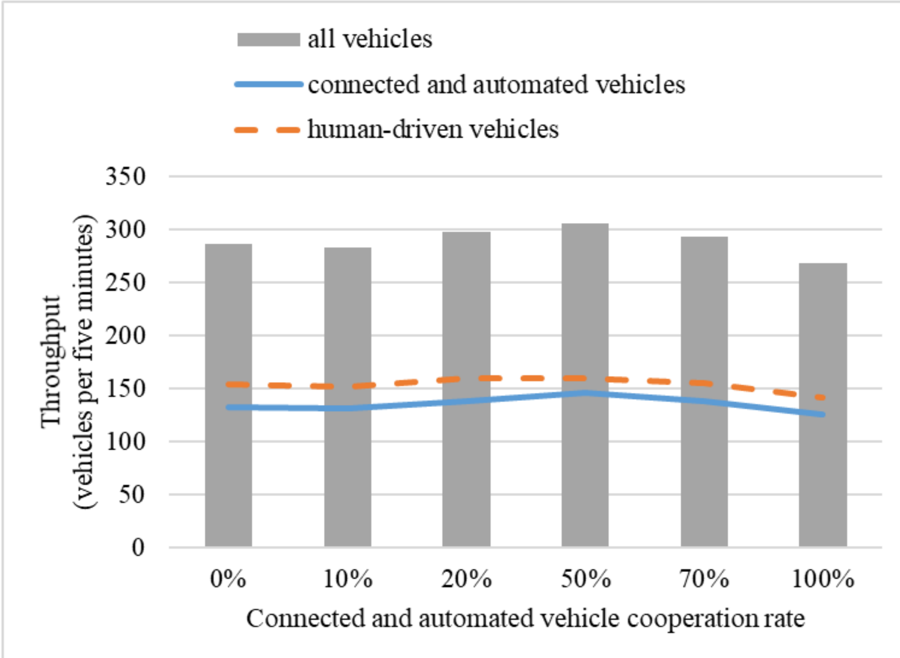

Source: FHWA.
% = percent.

(c) Throughput versus connected and automated vehicle cooperation rate.

Figure 40. Graph. Sensitivity analysis on connected and automated vehicle cooperation rate under congested traffic.

A shown in Figure 40, as CAV cooperation rate φ increased, the mobility and stability performance improved initially (φ <50 percent). This was probably because as φ initially increased, the traffic stream was more cooperative (i.e., this increased the chance of CAVs completing LCs quickly). This reduced the impedance from downstream LCs to upstream vehicle movements. However, the traffic performance degraded as φ further increased (φ >50 percent). This is probably because many LCs are incentivized by a high cooperation rate. Overly frequent LCs consequentially increase the average gaps between vehicles and create more oscillatory vehicle speeds, which lead to slower and less stable traffic.

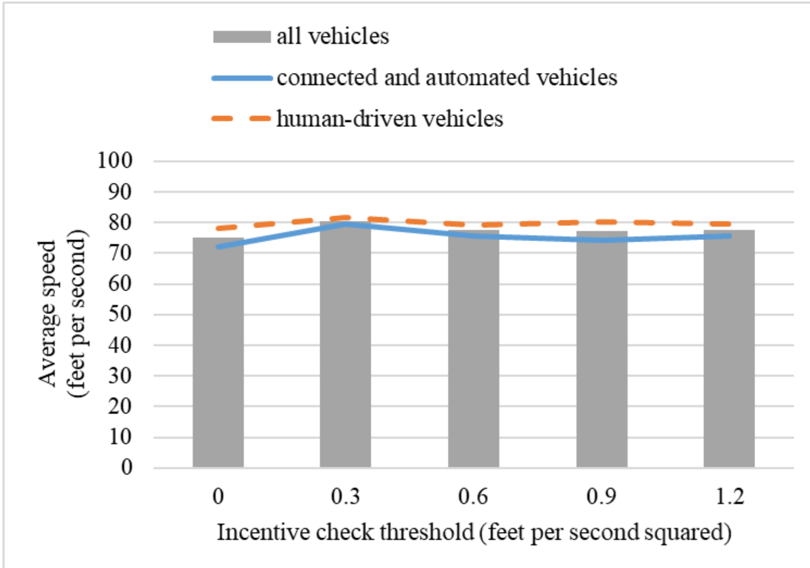

Source: FHWA.

(a) Average speed versus incentive criterion threshold.

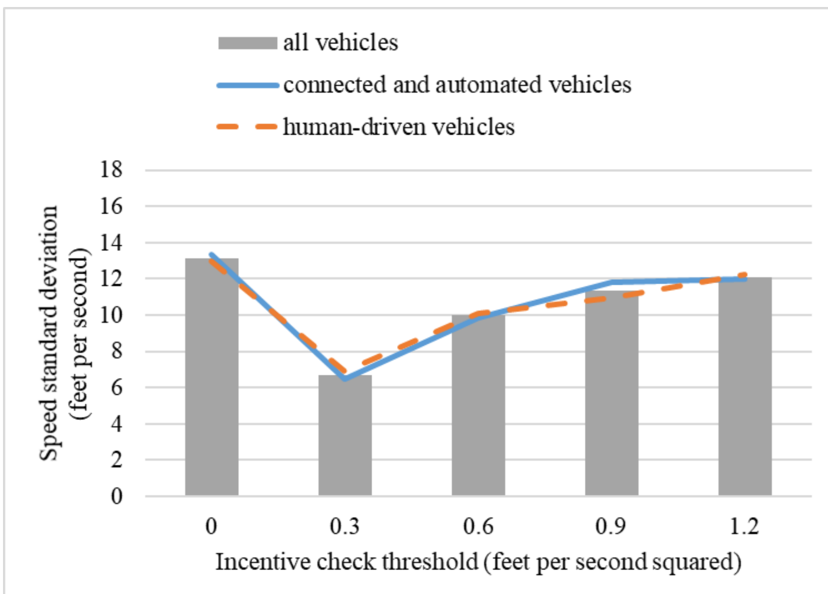

Source: FHWA.

(b) Speed standard deviation versus incentive criterion threshold.

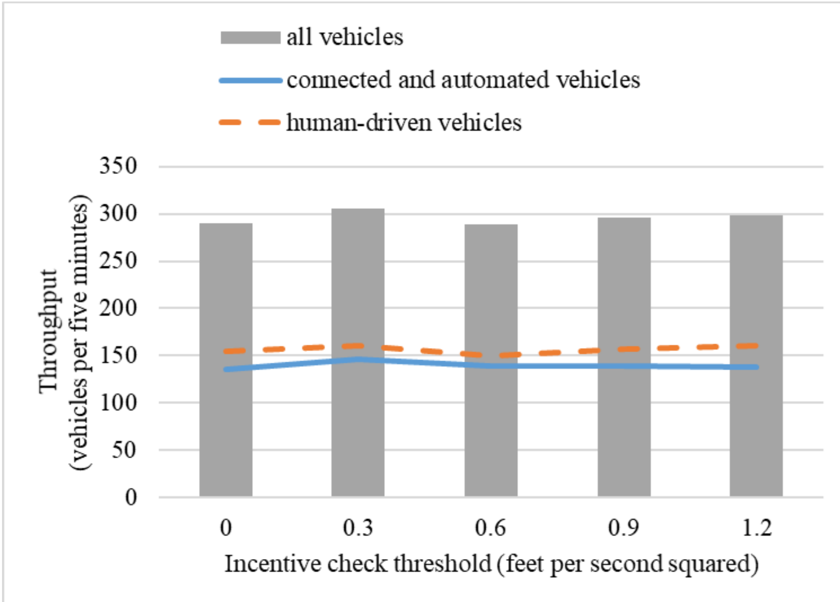

Source: FHWA.

(c) Throughput versus incentive criterion threshold.

Figure 41. Graph. Sensitivity analysis on incentive criterion threshold under congested traffic.

As the incentive criterion threshold Δa increased, both mobility and stability initially improved and then worsened. The pivot point was observed at $\Delta a = 0.3$ ft/s^2. Interestingly, this pivot Δa value was consistent with the typical value for the HV LC model suggested in the existing study (Treiber and Kesting, 2013), indicating that human drivers might have subconsciously learned the optimal LC behavior through extensive driving experience. As Δa increased, the CAV discretionary lane change (DLC) incentive criterion became more difficult to meet, leading to less DLC behaviors. At first, fewer DLC behaviors led to less traffic oscillation and thus contributed to better traffic performance. However, as Δa increased, DLCs became quite rare and many CAVs stuck to a slower speed rather than attempting to change to a faster lane. This held vehicles moving slower overall and thus deteriorated traffic performance (Li et al. 2006).

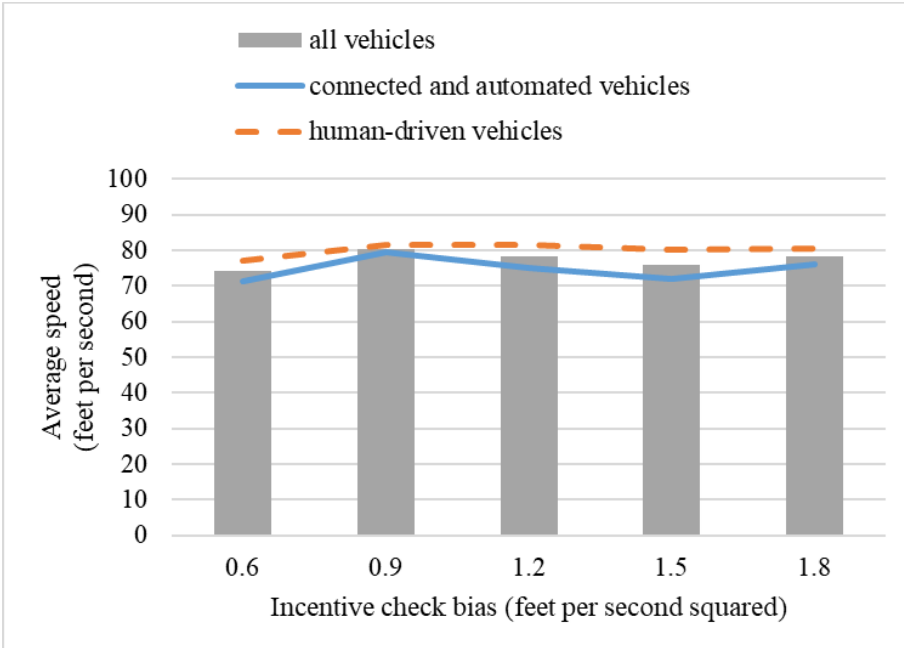

Source: FHWA.

(a) Average speed versus incentive criterion bias.

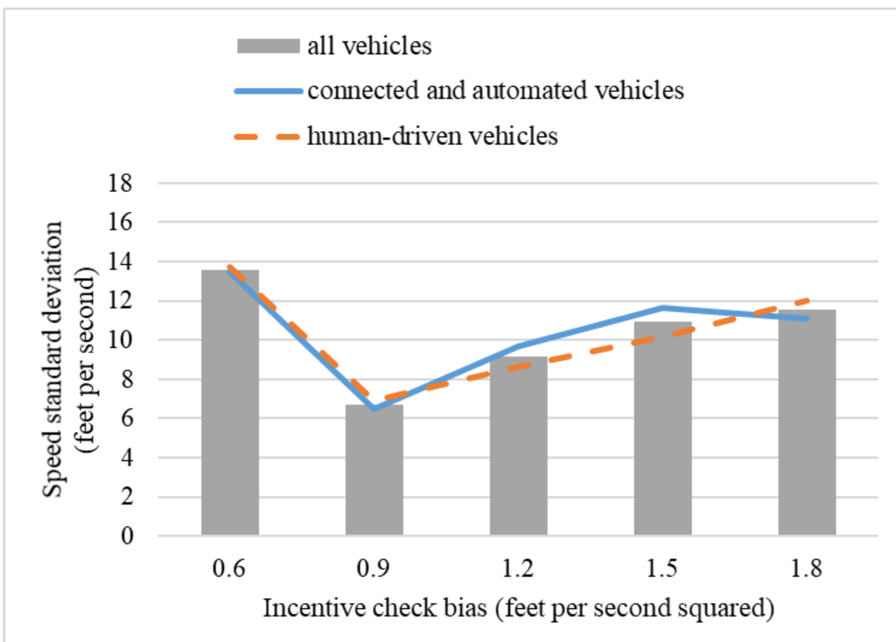

Source: FHWA.

(b) Speed standard deviation versus incentive criterion bias.

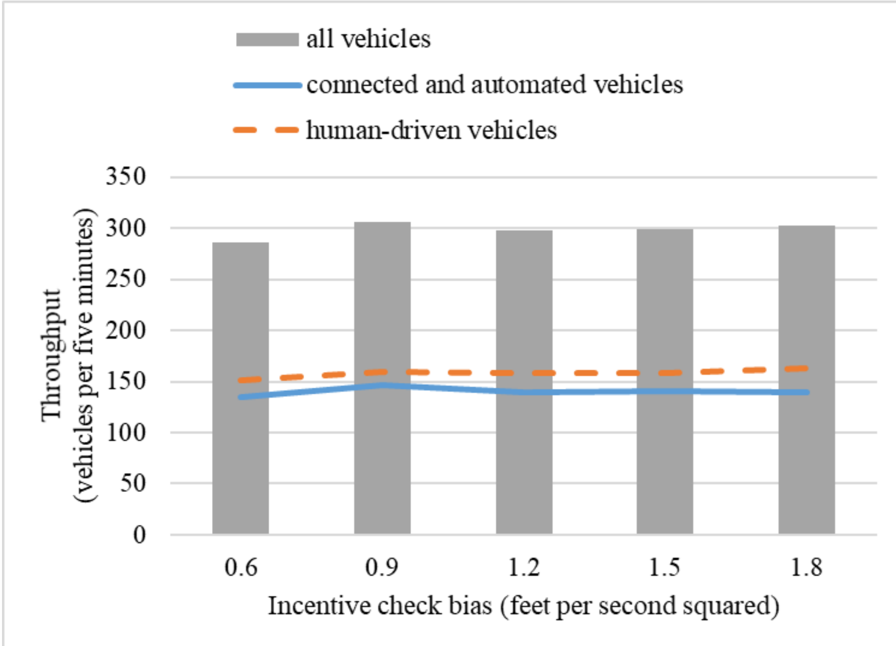

Source: FHWA.

(c) Throughput versus incentive criterion bias.

Figure 42. Graph. Sensitivity analysis on incentive criterion bias under congested traffic.

Again, as the incentive criterion bias a_{bias} (the tendency for a vehicle to stay in a right lane) increased, both mobility and stability performance first improved and then worsened. The best system performance was observed when a_{bias} = 0.9 ft/s^2. Interestingly, this value is again consistent with the typical value for HVs suggested in the existing study (Treiber and Kesting, 2013), suggesting the optimal human driver learning capability. The reasons to observe this trend were probably because as a_{bias} initially increased, congestion in the left lanes decreased, allowing more vehicles to overtake at faster speeds in the left lanes. However, as a_{bias} further increased, vehicles disproportionally concentrated in the right lanes, which impeded on-ramp traffic, and aggravated overall congestion.

Sensitivity Analysis Results of Uncongested Traffic

As shown in Figure 43, Figure 44, Figure 45, and Figure 46, mobility and stability performance under uncongested traffic were better than those under congested traffic in general. This is intuitive because traffic congestion degrades the traffic performance. Overall, the trends of the impacts were consistent with those in the congested traffic. However, a closer look reveals that the traffic performance (i.e., the average speed, the speed standard deviation, or the throughput) varies in a smaller range compared with that in Figure 39, Figure 40, Figure 41, and Figure 42. This indicates that the influence of the parameters' values on traffic became marginal as the traffic volume decreased (i.e., uncongested traffic). This is probably because in uncongested traffic, vehicles have more room to maneuver around to mitigate impacts from surrounding LC vehicles. From another angle, these findings indicate that the impacts will be amplified in more congested traffic, and thus more efforts are necessary in managing congested mixed traffic.

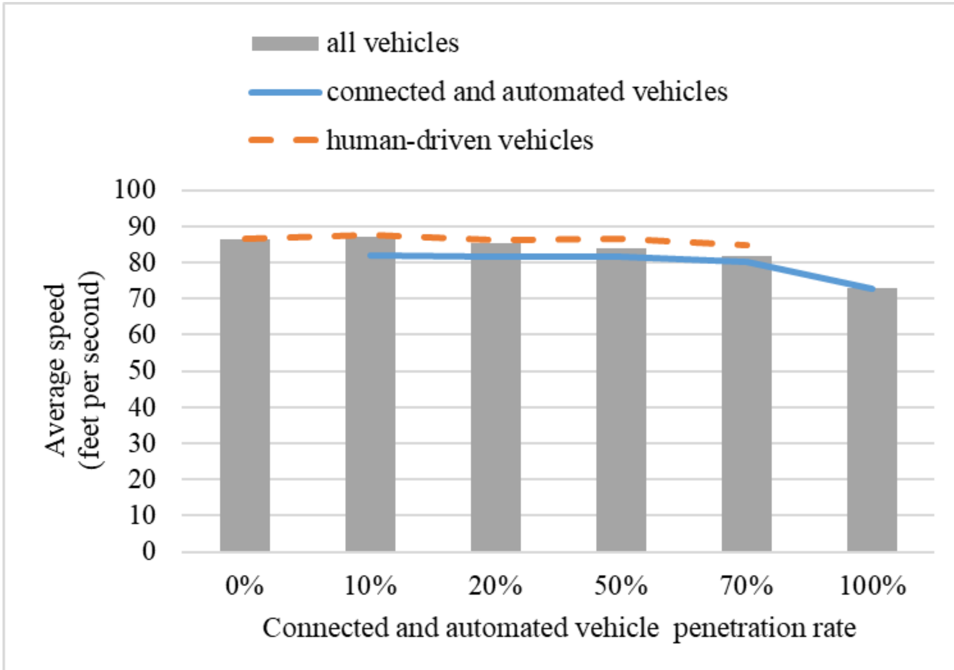

Source: FHWA.
% = percent.

(a) Average speed versus connected and automated vehicle penetration rate.

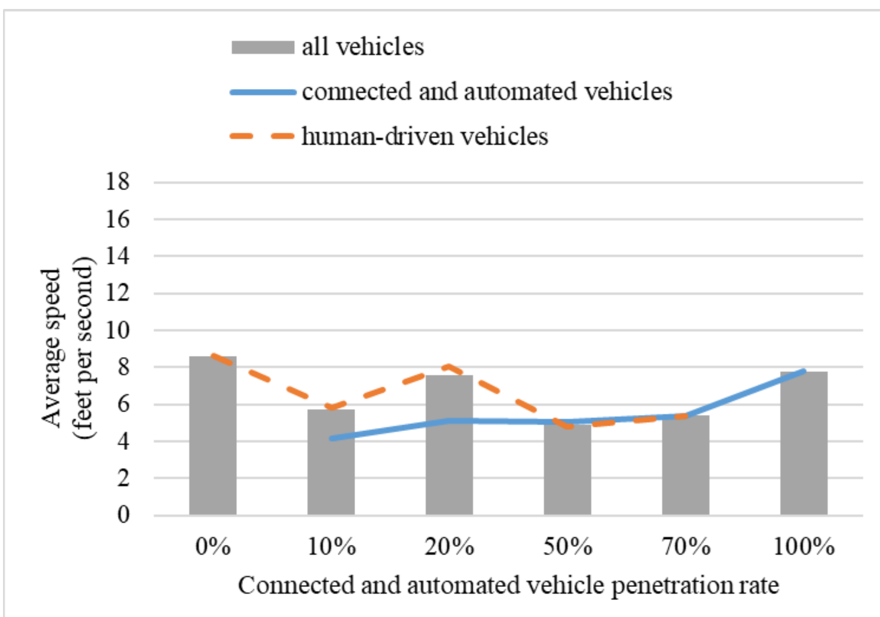

Source: FHWA.
% = percent.

(b) Speed standard deviation versus connected and automated vehicle penetration rate.

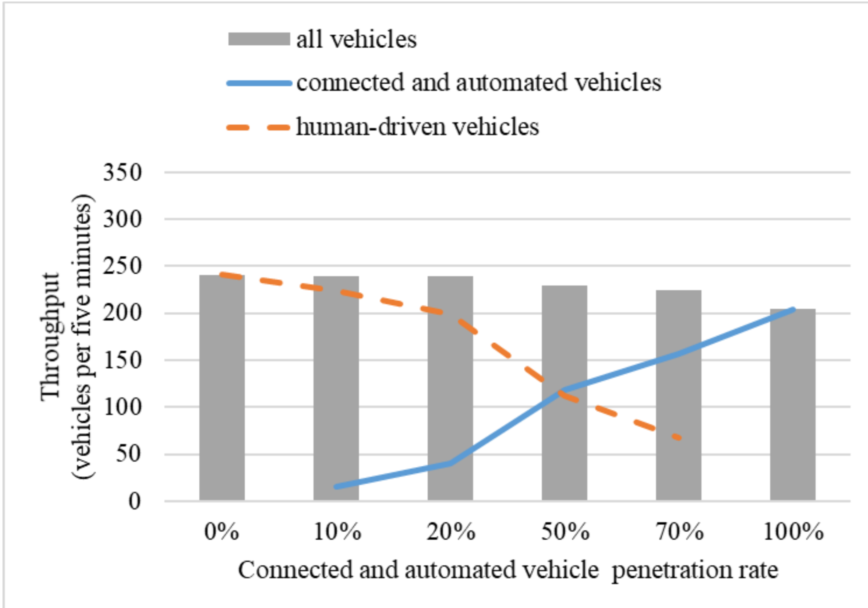

Source: FHWA.
% = percent.

(c) Throughput versus connected and automated vehicle penetration rate.

Figure 43. Graph. Sensitivity analysis on connected and automated vehicle penetration rate under uncongested traffic.

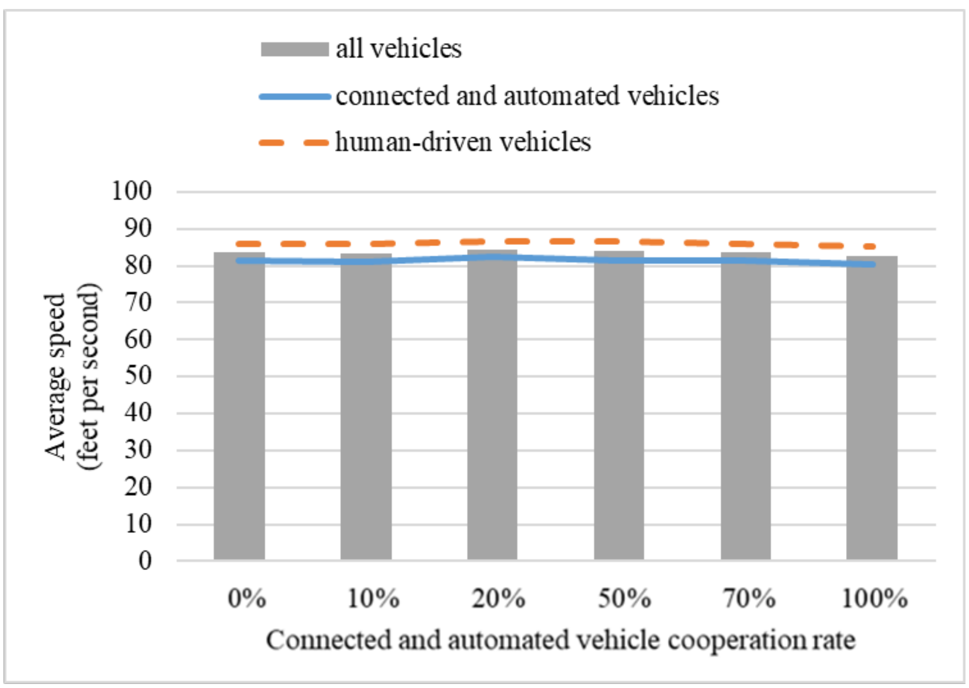

Source: FHWA.
% = percent.

(a) Average speed versus connected and automated vehicle cooperation rate.

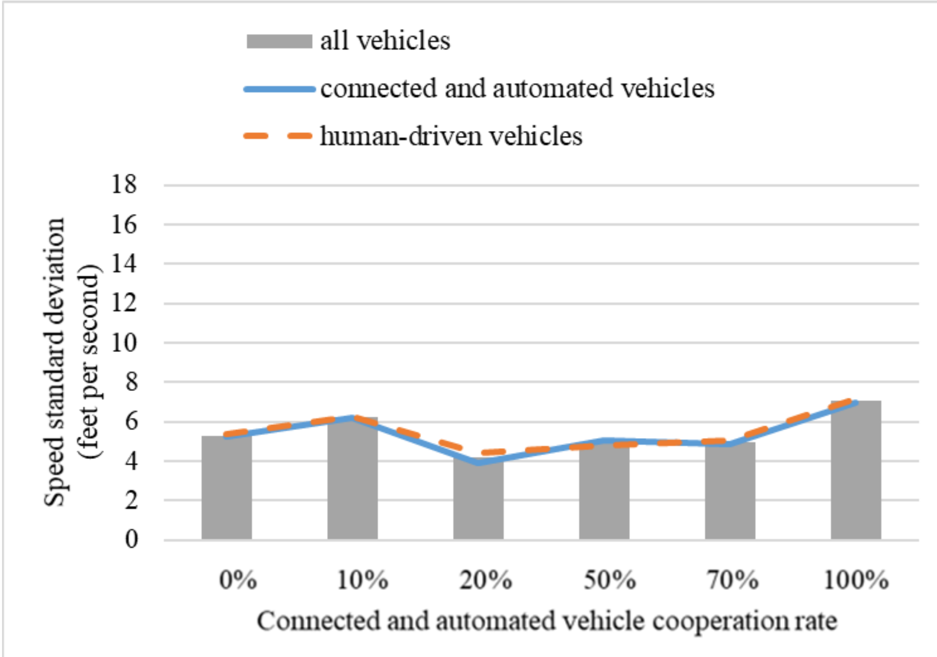

Source: FHWA.
% = percent.

(b) Speed standard deviation versus connected and automated vehicle cooperation rate.

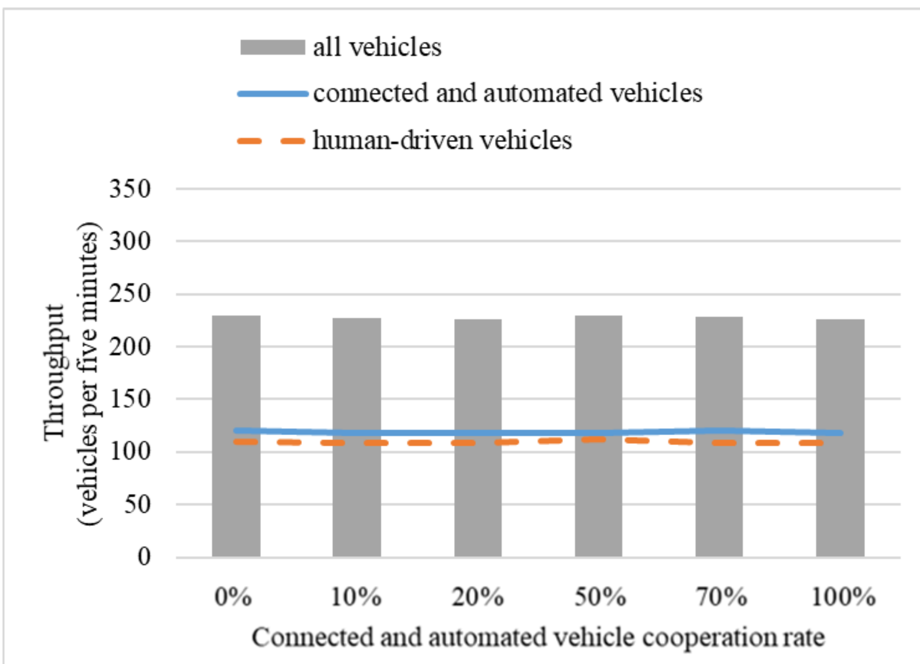

Source: FHWA.
% = percent.

(c) Throughput versus connected and automated vehicle cooperation rate.

Figure 44. Graph. Sensitivity analysis on connected and automated vehicle cooperation rate under uncongested traffic.

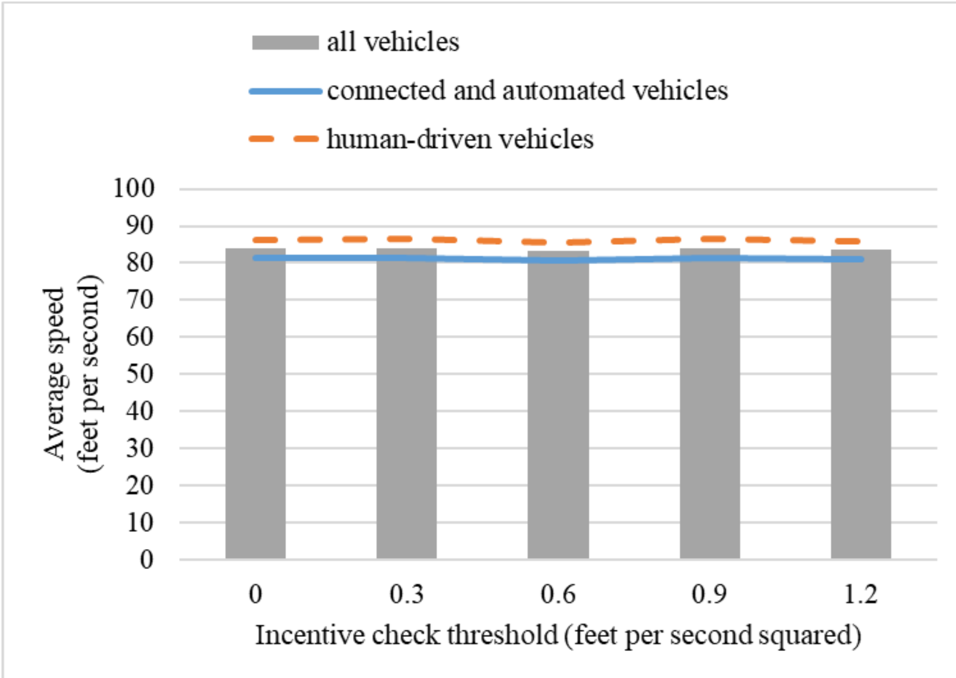

Source: FHWA.

(a) Average speed versus incentive criterion threshold.

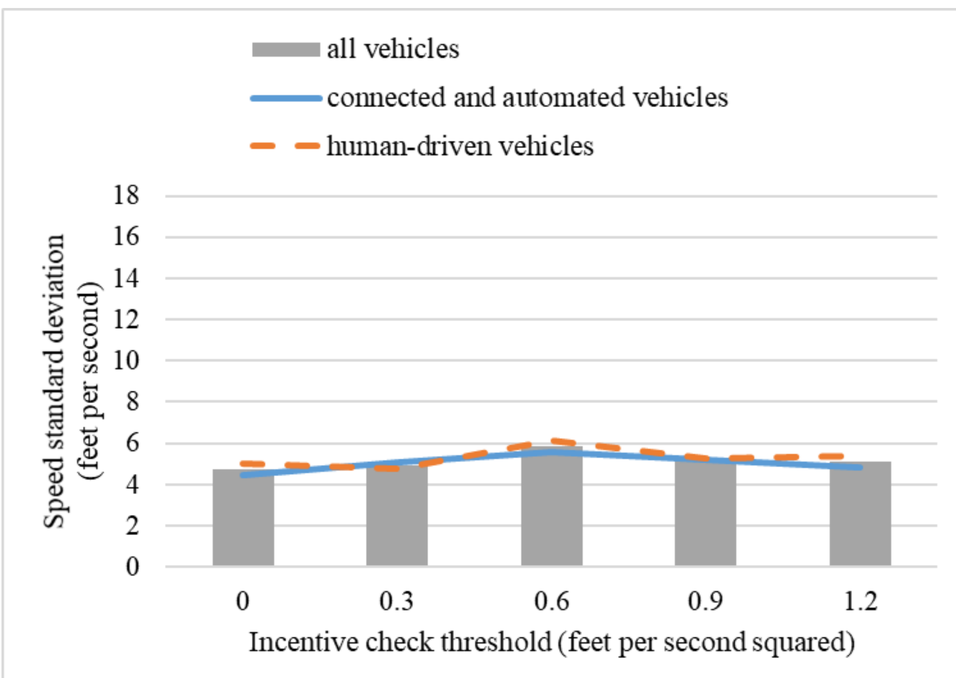

Source: FHWA.

(b) Speed standard deviation versus incentive criterion threshold.

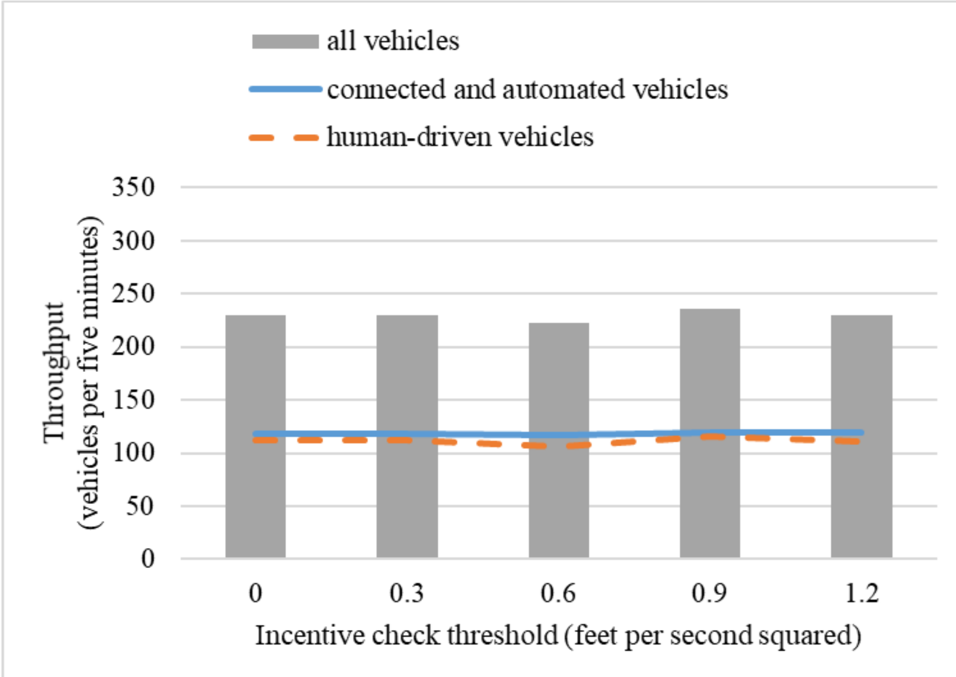

Source: FHWA.

(c) Throughput versus incentive criterion threshold.

Figure 45. Graph. Sensitivity analysis on incentive criterion threshold under uncongested traffic.

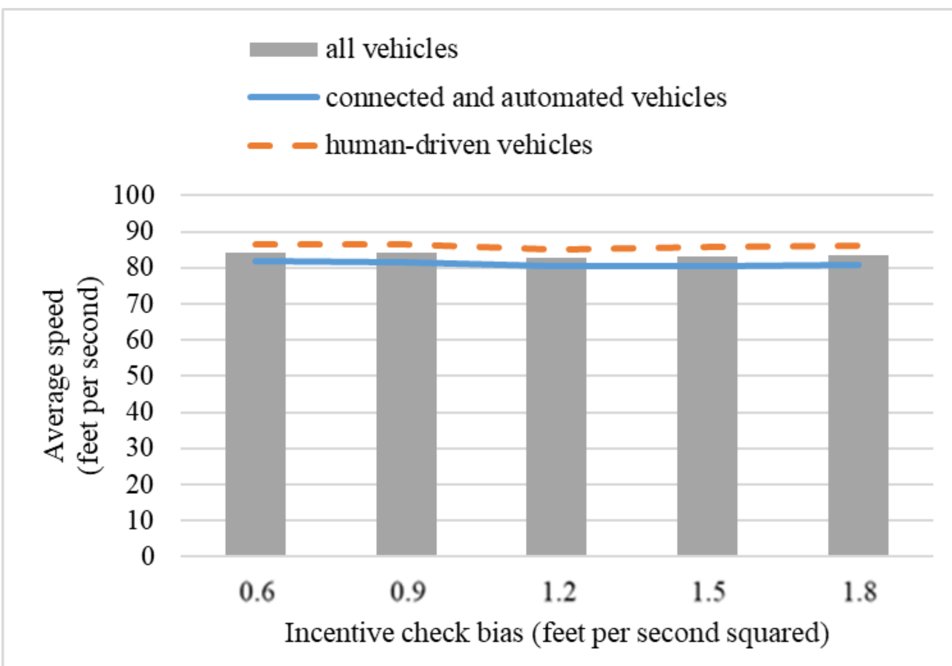

Source: FHWA.

(a) Average speed versus incentive criterion bias.

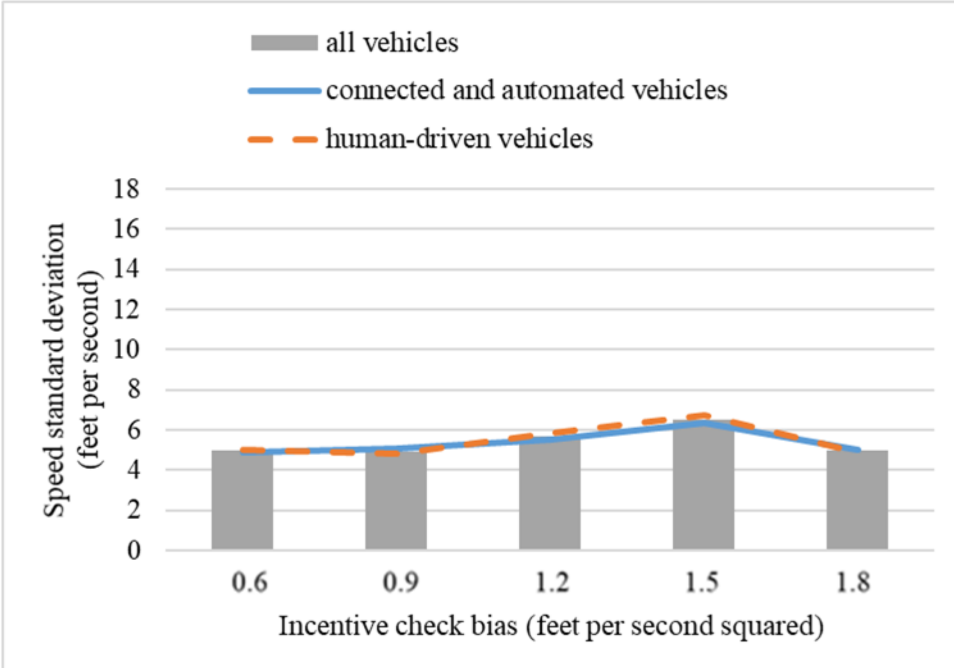

Source: FHWA.

(b) Speed standard deviation versus incentive criterion bias.

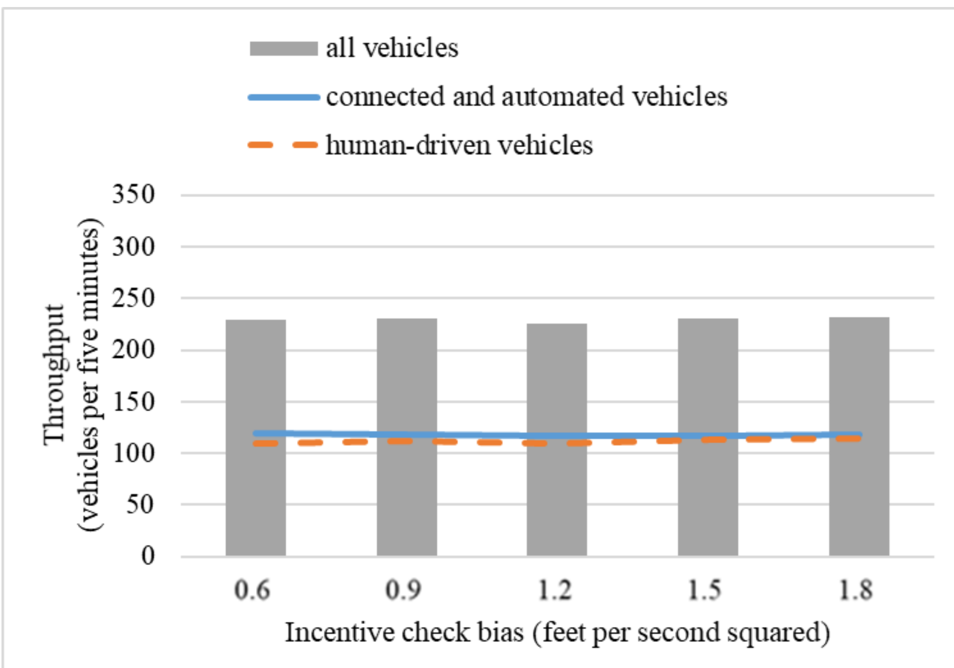

Source: FHWA.

(c) Throughput versus incentive criterion bias.

Figure 46. Graph. Sensitivity analysis on incentive criterion bias under uncongested traffic.

Overall, note that the impacts of several key parameters (e.g., CAV cooperation rate) LC incentive criterion threshold and bias on traffic performance are nonlinear (e.g., first improving and then degrading). These findings indicate that thoughts on optimization may be taken when designing these parameters from the perspective of transportation operators (e.g., facilities and policies to promote vehicle cooperation) and automakers (e.g., tuning parameters in their LC models) to achieve the best traffic performance. These insights may help stakeholders better understand and prepare for near-future mixed CAV traffic with different LC behaviors and also suggests the optimal LC configurations for automakers to achieve the best overall traffic performance.

CHAPTER 6. SUMMARY AND RECOMMENDATIONS

This chapter described a mixed traffic simulation framework that is centered at the CAV LC model and fully considers the dynamics of surrounding vehicles under different mixed traffic scenarios. The model was calibrated and validated using data collected from a small-scale field experiment. The model is open source and can be customized and implemented into existing microsimulation simulators to meet different application requirements in the future. For the purposes of this project, PTV Vissim was adopted as an example to implement the model and a case study was conducted on the I–75 highway segment. The results from sensitivity analyses on key parameters revealed:

1. The mobility performance was affected by the CAV headway in relation to the HV headway. In the case that the CAV headway was longer (which is possible in the initial stage of CAV deployment), the mobility performance degraded with the CAV penetration rate increased.

2. The overall traffic performance initially improved and then degraded as the cooperation rate increased. This is probably because too low cooperation rates would have decreased the chances for CAVs to complete LCs, and thus the CAVs remained at a slower speed for longer. On the other hand, too high cooperation rates would have resulted in greater vehicle gaps and more speed oscillation due to overly frequent LC activities.

3. As incentive criterion threshold Δa increased, similarly, the traffic performance initially improved and then degraded. This is probably because too low Δa values would have encouraged overly frequent DLCs that, again, would have increased vehicle gaps and speed oscillation. On the other hand, too high Δa values would have decreased the chances of DLCs, and thus cause vehicles to be stuck at slower speeds.

4. As incentive criterion bias a_{bias} increased, similarly, the traffic performance initially improved and then degraded. This is probably because too low a_{bias} values would have resulted in more vehicles in the left lanes, thus blocking fast overtaking vehicles. On the other hand, too high a_{bias} would have led to disproportionally heavy traffic concentration in the right lanes, which would have impeded on-ramp traffic and aggravate overall congestion.

5. The optimal Δa and a_{bias} values for the best performance were consistent with those observed in the existing HV traffic. This indicated that human drivers, to some extent, might have learned the optimal driving behavior. Thus, the design of CAV driving models might benefit from learning HV driving behavior.

6. The impacts were amplified as the traffic congestion level increased, probably because vehicles in more congested traffic would have had less room to maneuver through against downstream LC activities.

The proposed model is limited in the following aspects: First, the calibration and validation approaches were performed with the field data from relatively small-scale experiments with a specific lab-designed automated vehicle. These approaches may be tested with larger-scale data with more diverse CAV technologies. Second, platooning for longitudinal CAV control is not considered in the study. Third, various HV behaviors in response to surrounding CAVs as indicated from previous studies (e.g., Zhao et al. 2020) are not yet incorporated.

REFERENCES

Gipps, P.G., 1981. A behavioural car-following model for computer simulation. Transportation Research Part B: Methodological 15, 105–111.

Gunter, G., Janssen, C., Barbour, W., Stern, R., Work, D., 2019. Model based string stability of adaptive cruise control systems using field data. IEEE Transactions on Intelligent Vehicles.

Hamdar, S.H., Dixit, V. V, Talebpour, A., Treiber, M., 2019. A behavioral microeconomic foundation for car-following models. Transportation Research Part C: Emerging Technologies.

Li, B., Zhang, Youmin, Feng, Y., Zhang, Yue, Ge, Y., Shao, Z., 2018. Balancing computation speed and quality: A decentralized motion planning method for cooperative lane changes of connected and automated vehicles. IEEE Transactions on Intelligent Vehicles 3, 340–350.

Li, X.-G., Jia, B., Gao, Z.-Y., Jiang, R., 2006. A realistic two-lane cellular automata traffic model considering aggressive lane-changing behavior of fast vehicle. Physica A: Statistical Mechanics and its Applications 367, 479–486.

Lu, X., Liu, H., Li, X., Li, Q., Mahmassani, H., Talebpour, A., Hosseini, M., Huang, Z., Hale, D. K., and Shladover, S. E. (Forthcoming). Developing Analysis, Modeling, and Simulation Tools for Connected and Automated Vehicle Applications. FHWA.

Milanés, V., Shladover, S.E., 2014. Modeling cooperative and autonomous adaptive cruise control dynamic responses using experimental data. Transportation Research Part C: Emerging Technologies 48, 285–300.

PTV Group. 2018. PTV Vissim. https://www.ptvgroup.com/en/solutions/products/ptv-vissim/.

Microsoft Visual Studio®. 2019. https://visualstudio.microsoft.com/

Smith, B.W., 2013. SAE levels of driving automation. Center for Internet and Society. Stanford Law School. http://cyberlaw. stanford. edu/blog/2013/12/sae-levels-drivingautomation.

Treiber, M., Kesting, A., 2013. Traffic flow dynamics. Traffic Flow Dynamics: Data, Models and Simulation, Springer-Verlag Berlin Heidelberg.

Wang, Z., Zhao, X., Xu, Z., Li, X., Qu, X., 2020. Modeling and Field Experiments on Lane Changing of an Autonomous Vehicle in Mixed Traffic. Computer-aided Civil and Infrastructure Engineering.

Xiao, L., Gao, F., 2010. A comprehensive review of the development of adaptive cruise control systems. Vehicle system dynamics 48, 1167–1192.

Xu, G., Liu, L., Ou, Y., Song, Z., 2012. Dynamic modeling of driver control strategy of lane-change behavior and trajectory planning for collision prediction. IEEE Transactions on Intelligent Transportation Systems 13, 1138–1155.

Zhao, X., Wang, Z., Xu, Z., Wang, Y., Li, X., Qu, X., 2020. Field experiments on longitudinal characteristics of human driver behavior following an autonomous vehicle. Transportation Research Part C: Emerging Technologies 114, 205–224.

APPENDIX – PSEUDOCODE

MAIN PROGRAM

Initialize vehicles $n \in [1 \ldots N]$ (including both connected autonomous vehicles (CAVs) and human driven vehicles (HVs)) with their routes. And set CAV cooperation states. Set simulation duration T and start the simulation.

```
for t ϵ [0, T]
    for n ϵ [1, N]
        if vehicle n is HV
            update n position with customized HV car-following (CF) and lane-changing (LC)
            rules [1]
        else if vehicle n is CAV
            if is at lane keeping state
                keep following on CF path [2]
                    if n is cooperative and preceding CAV(s) in the adjacent lane (s)
                LC signal (s) is (are) on
                        n will follow the preceding vehicle in the current lane and
                        preceding CAV(s) in the adjacent lane (s) using ACC
                        model. i.e., conducting cooperative CF [3]
                    else
                        n will only follow the preceding vehicle in the current lane
                        using ACC model and ignore preceding CAV(s) LC
                        signal (s) in the adjacent lane (s), i.e., conducting
                        uncooperative CF [4]
                    end
            else if n is during a LC process
                if n has not passed the lane marking
                    if safety check passes [5]
                        set LC path and follow LC path [6]
                            n will follow the preceding vehicles in the current
                            and target lane using ACC model [7].
                    else
                        set LC abortion path and follow LC abortion path [8]
                            n will only follow the preceding vehicle in the
                            current lane using ACC model and go back to the
                            center line of the current lane [9]
                else
                    set LC path and follow LC path [6]
                        n will only follow the preceding vehicle in the target lane
                    using ACC model [10].
                end
            else if i is at discretionary LC check state
                if incentive check passes [11]
                    if safety check passes [5]
                        set LC path and follow LC path [6]
                            n will follow the preceding vehicles in the current
                            and target lane using ACC model [7]
                    else
                        set LC abortion path and follow LC abortion path [8]
```

n will only follow the preceding vehicle in the current lane using ACC model and go back to the center line of the current lane [9]
end
else
keep following on CF path [2]
if *n* is cooperative and preceding CAV(s) in the adjacent lane (s) LC signal (s) is (are) on
n will follow the preceding vehicle in the current lane and preceding CAV(s) in the adjacent lane (s) using ACC model. i.e., conducting cooperative CF [3]
else
n will only follow the preceding vehicle in the current lane using ACC model and ignore preceding CAV(s) LC signal (s) in the adjacent lane (s), i.e., conducting uncooperative CF [4]
end
end
else if *n* is at mandatory LC check state
if safety check passes [5]
set LC path and follow LC path [6]
n will follow the preceding vehicles in the current and target lane using ACC model [7]
else
set LC abortion path and follow LC abortion path [8]
n will only follow the preceding vehicle in the current lane using ACC model and go back to the center line of the current lane [9]
end
else if *n* is at LC abortion state
keep following on LC abortion path [8]
end
end
end
end

FUNCTIONS

[1] Update HV position with customized HV CF/LC rules

Description: This study mainly focuses on the CAV control and different HV control rules can be adopted into the mixed traffic simulation framework to control HVs per application needs, such as the intelligent driver model and Newell's CF model.

[2] CF path

Description: The center line of a lane is set as the CAV CF path (the red dashed line), shown in Figure 3.

[3] Cooperative CF on CF path

Description: When a CAV is at CF state and cooperative, and the CAV(s) in the adjacent lane(s) (i.e., vehicle 2 in Figure 4 [b]) is (are) having the LC signal(s) on to make LC(s) to the front of this CAV, this CAV will start cooperative CF on the CF path. It will yield to the LC CAV(s) by using linear adaptive cruise control (ACC) model to follow the current preceding vehicle (i.e., vehicle 1 in Figure 4 [b]) and the LC CAV(s) (i.e., vehicle 2 in Figure 4 [b]).

Formulation:

$$\tilde{a}^1{}_{\mathrm{CAV}}(t) = K_1(x_1(t) - x_{\mathrm{CAV}}(t) - C - v_{\mathrm{CAV}}(t)g_{\mathrm{CAV}}) + K_2\big(v_1(t) - v_{\mathrm{CAV}}(t)\big), \forall t \in \mathcal{T}$$

$$\tilde{a}^2{}_{\mathrm{CAV}}(t) = K_1(x_2(t) - x_{\mathrm{CAV}}(t) - C - v_{\mathrm{CAV}}(t)g_{\mathrm{CAV}}) + K_2\big(v_2(t) - v_{\mathrm{CAV}}(t)\big), \forall t \in \mathcal{T},$$

$$\tilde{a}_{\mathrm{CAV}}(t) = \min\{\tilde{a}^1{}_{\mathrm{CAV}}(t), \tilde{a}^2{}_{\mathrm{CAV}}(t)\}.$$

Input:

K_1, K_2: the parameters of the linearized ACC model

g_{CAV}: the desired time gap of CAV

C: the length of the vehicle (CAV and HV)

$x_{\mathrm{CAV}}(t)$: the longitude position of the CAV at time t.

$v_{\mathrm{CAV}}(t)$: the speed of the CAV at time t.

$x_1(t)$: the longitude position of vehicle 1 at time t.

$x_2(t)$: the longitude position of vehicle 2 at time t.

$v_1(t)$: the speed of vehicle 1 at time t.

$v_2(t)$: the speed of vehicle 2 at time t.

Output:

$\tilde{a}_{\mathrm{CAV}}(t)$: the acceleration of the CAV following vehicle 1 and vehicle 2 on the CF path

[4] Uncooperative CF on CF path

Description: When a CAV is at CF state and uncooperative, and the CAV(s) in the adjacent lane(s) (i.e., vehicle 2 in Figure 4 [a]) is(are) having the LC signal(s) on to make LC(s) to the front of this CAV, this CAV will conduct uncooperative CF by using linearized ACC model to follow the current preceding vehicle (i.e., vehicle 1 in Figure 4 [a]) and ignoring the LC signal(s).

Formulation:

$$\tilde{a}_{\text{CAV}}(t) = K_1(x_1(t) - x_{\text{CAV}}(t) - C - v_{\text{CAV}}(t)g_{\text{CAV}}) + K_2\big(v_1(t) - v_{\text{CAV}}(t)\big), \forall t \in \mathcal{T}$$

Input:

K_1, K_2: the parameters of the linearized ACC model

g_{CAV}: the desired time gap of CAV

C: the length of vehicle

$x_{\text{CAV}}(t)$: the longitude position of the CAV at time t

$v_{\text{CAV}}(t)$: the speed of the CAV at time t

$x_1(t)$: the longitude position of vehicle 1 at time t

$v_1(t)$: the speed of vehicle 1 at time t

Output:

$\tilde{a}_{\text{CAV}}(t)$: the acceleration of the CAV following vehicle 1 on the CF path

[5] Safety check

Description: There are two components in the safety check. The first check is to check the distance between the CAV position and the preceding vehicle (i.e., vehicle 2 in Figure 12) position in the target lane when the LC is finished. This distance is compared with the expected minimum safety distance calculated by Gipps' safe distance algorithm. If the distance between the CAV and vehicle 2 is no less than the minimum safety distance, the CAV LC will not cause too dramatic deceleration to the CAV, and hence the safety check with respect to vehicle 2 passes. The second check is for the following vehicle (i.e., vehicle 3 in Figure 12) on the target lane. Intelligent driver model (IDM) is used to calculate the target acceleration of the following vehicle in the target lane. If the following vehicle's target acceleration is greater than the maximum deceleration, the CAV LC maneuver will not cause too dramatic deceleration to vehicle 3, and hence the safety check concerning vehicle 3 passes. If both these two components passed, the safety check passes.

Formulation:

$$S(t) = v_{\text{CAV}}(t)\tau_{\text{CAV}} + \frac{\big(v_{\text{CAV}}(t)\big)^2}{2b_{\text{CAV}}} - \frac{\big(\hat{v}_2(t)\big)^2}{2\hat{b}_2}, \forall t \in \mathcal{T}$$

Where τ_{CAV} is the reaction time of the CAV, b_{CAV} is the maximum deceleration of the CAV, $\hat{v}_2(t)$ is the speed of vehicle 2 at time t, $\hat{x}_2(t)$ is the longitude position of vehicle 2 at time t,

$$\hat{a}_3(t) = \widehat{w}_3\left[1 - \left(\frac{\hat{v}_3(t)}{v_{\text{CAV}}(t)}\right)^{\delta} - \left(\frac{S^*(\hat{v}_3(t), \Delta v(t))}{\hat{S}(t)}\right)^2\right], \forall t \in \mathcal{T}$$

$$S^*(\hat{v}_3(t), \Delta v(t)) = s_0 + \max\left(0, \hat{v}_3(t)\Delta\mathrm{T} + \frac{\hat{v}_3(t)\big(v_{\text{CAV}}(t) - \hat{v}_3(t)\big)}{2\sqrt{-\widehat{w}_3\hat{b}_3}}\right), \forall t \in \mathcal{T}$$

$$\hat{S}(t) = x_{\text{CAV}}(t) - \hat{x}_3(t) - C, \forall t \in \mathcal{T},$$

Input:

τ_{CAV}: the reaction time of CAV

b_{CAV}: the maximum deceleration of CAV

$\hat{v}_2(t)$: the speed of vehicle 2 at time t

$\hat{b}_2$: the maximum deceleration of vehicle 2

s_0: the minimum gap

ΔT: the time gap

δ: the acceleration exponent

$\hat{w}_3$: the maximum acceleration of vehicle 3

$\hat{b}_3$: the maximum deceleration of vehicle3

Output:

Whether the safety check passes or not

[6] LC path

Description: After the needed checks pass, a linear function LC path (i.e., the red solid line in Figure 12) is used to replace the sine-function based LC path (i.e., the black dotted curve in Figure 12) to improve the simulation efficiency in the local coordinate system.

Formulation:

$$y'_{\mathrm{CAV}}(t) = y_{\mathrm{CAV}}(t) + \frac{R^{\mathrm{Y}}(t)}{R^{X}(t)}\left(x'_{\mathrm{CAV}}(t) - x_{\mathrm{CAV}}(t)\right), x'_{\mathrm{CAV}} \in [x_{\mathrm{CAV}}(t), x_2(t) - S(t) - C], \forall t \in \mathcal{T}$$

$$R^{\mathrm{X}}(t) = x_2(t) - S(t) - x_{\mathrm{CAV}}(t) - C, \forall t \in \mathcal{T}$$

$$R^{\mathrm{Y}}(t) = y_{\mathrm{CAV}}(t) - y_2(t), \forall t \in \mathcal{T}$$

Input:

$x_{\mathrm{CAV}}(t)$: the longitudinal position of the CAV at time t.

$y_{\mathrm{CAV}}(t)$: the latitudinal position of the CAV at time t.

$x_2(t)$: the longitudinal position of vehicle 2 at time t.

$y_2(t)$: the latitudinal positions of vehicle 2 at time t.

$S(t)$: the safety distance calculated in Figure 8.

C: the vehicle length

$R^{\mathrm{X}}(t)$: the longitudinal gap between the CAV and vehicle 2 at time t.

$R^{\mathrm{Y}}(t)$: the lateral offset between the CAV and vehicle 2 at time t.

Output:

A smooth LC path at time t composed of discrete points (x'_{AV}, y'_{AV}) in the local coordinate system

[7] CF on LC path (before passing lane marking)

Description: Before a CAV passes the lane marking, it uses linearized ACC model to follow the both preceding vehicles in the current lane (i.e., vehicle 1 in Figure 13 [a]) and the target lane (i.e., vehicle 2 in Figure 13 [a]).

Formulation:

$$\tilde{a}^1{}_{\mathrm{CAV}}(t) = K_1(x_1(t) - x_{\mathrm{CAV}}(t) - C - v_{\mathrm{CAV}}(t)g_{\mathrm{CAV}}) + K_2\left(v_1(t) - v_{\mathrm{CAV}}(t)\right), \forall t \in \mathcal{T}$$

$$\tilde{a}^2{}_{\mathrm{CAV}}(t) = K_1(x_2(t) - x_{\mathrm{CAV}}(t) - C - v_{\mathrm{CAV}}(t)g_{\mathrm{CAV}}) + K_2\left(v_2(t) - v_{\mathrm{CAV}}(t)\right), \forall t \in \mathcal{T},$$

$$\tilde{a}_{\mathrm{CAV}}(t) = \min\{\tilde{a}^1{}_{\mathrm{CAV}}(t), \tilde{a}^2{}_{\mathrm{CAV}}(t)\}.$$

Input:

K_1, K_2: the parameters of the linearized ACC model.

g_{CAV}: the desired time gap of CAV.

C: the length of the vehicle (CAV and HV).

$x_{\text{CAV}}(t)$: the longitude position of the CAV at time t.

$v_{\text{CAV}}(t)$: the speed of the CAV at time t.

$x_1(t)$: the longitude position of vehicle 1 at time t.

$x_2(t)$: the longitude position of vehicle 2 at time t.

$v_1(t)$: the speed of vehicle 1 at time t.

$v_2(t)$: the speed of vehicle 2 at time t.

Output:

$\tilde{a}_{\text{CAV}}(t)$: the acceleration of the CAV following vehicle 1 and vehicle 2 on the LC path

[8] LC abortion path

Description: Whenever the safety check fails to pass before the CAV passes the lane marking, the LC will be aborted and a LC abortion path (the green dashed line in Figure 12), symmetric to the LC path, will be generated.

[9] CF on LC abortion path

Description: When the CAV LC abortion is initiated, the CAV will use linearized ACC model to follow vehicle 1 in Figure 14 on the LC abortion path until it goes back to the center line of the current lane.

Formulation:

$$\tilde{a}_{\text{CAV}}(t) = K_1(x_1(t) - x_{\text{CAV}}(t) - C - v_{\text{CAV}}(t)g_{\text{CAV}}) + K_2\big(v_1(t) - v_{\text{CAV}}(t)\big), \forall t \in \mathcal{T}$$

Input:

K_1, K_2: the parameters of the linearized ACC model.

g_{CAV}: the desired time gap of CAV.

C: the length of vehicle.

$x_{\text{CAV}}(t)$: the longitude position of the CAV at time t.

$v_{\text{CAV}}(t)$: the speed of the CAV at time t.

$x_1(t)$: the longitude position of vehicle 1 at time t.

$v_1(t)$: the speed of vehicle 1 at time t.

Output:

$\tilde{a}_{\text{CAV}}(t)$: the acceleration of the CAV following vehicle 1 on the LC abortion path

[10] CF on LC path (after passing lane marking)

Description: After a CAV passes the lane marking, it uses linearized ACC model to follow only the preceding vehicles in the target lane (i.e., vehicle 2 in Figure 13 [b]).

Formulation:

$$\tilde{a}_{\text{CAV}}(t) = K_1(x_2(t) - x_{\text{CAV}}(t) - C - v_{\text{CAV}}(t)g_{\text{CAV}}) + K_2\big(v_2(t) - v_{\text{CAV}}(t)\big), \forall t \in \mathcal{T}$$

Input:

K_1, K_2: the parameters of the linearized ACC model.

g_{CAV}: the desired time gap of CAV.

C: the length of the vehicle (CAV and HV).

$x_{\text{CAV}}(t)$: the longitude position of the CAV at time t.

$v_{\text{CAV}}(t)$: the speed of the CAV at time t.

$x_2(t)$: the longitude position of vehicle 2 at time t.

$v_2(t)$: the speed of vehicle 2 at time t.

Output:

$\tilde{a}_{\text{CAV}}(t)$: the acceleration of the CAV following vehicle 2 on the LC path

[11] Incentive check

Description: The incentive check is only needed for discretionary LCs. The CAV will check and compare the accelerations of following the preceding vehicle in the current lane (i.e., vehicle 1 in Figure 5 [a]) and the accelerations of following the preceding vehicle in the target lane (i.e., vehicle 2 in Figure 5 [a]) using linearized ACC model. The incentive check will pass only if the acceleration of the CAV following vehicle 2 is greater than that of the CAV following vehicle 1 by a certain amount.

Formulation:

$$\tilde{a}^2{}_{\mathrm{CAV}}(t) - \tilde{a}^1{}_{\mathrm{CAV}}(t) > \Delta a + a_{bias}$$

$$\tilde{a}^1{}_{\mathrm{CAV}}(t) = K_1(x_1(t) - x_{\mathrm{CAV}}(t) - C - v_{\mathrm{CAV}}(t)g_{\mathrm{CAV}}) + K_2\big(v_1(t) - v_{\mathrm{CAV}}(t)\big), \forall t \in \mathcal{T},$$

$$\tilde{a}^2{}_{\mathrm{CAV}}(t) = K_1(x_2(t) - x_{\mathrm{CAV}}(t) - C - v_{\mathrm{CAV}}(t)g_{\mathrm{CAV}}) + K_2\big(v_2(t) - v_{\mathrm{CAV}}(t)\big), \forall t \in \mathcal{T},$$

Input:

K_1, K_2: the parameters of the linearized ACC model

g_{CAV}: the desired time gap of CAV

C: the length of the vehicle (CAV and HV)

$x_{\mathrm{CAV}}(t)$: the longitude position of the CAV at time t.

$v_{\mathrm{CAV}}(t)$: the speed of the CAV at time t.

$x_1(t)$: the longitude position of vehicle 1 at time t.

$x_2(t)$: the longitude position of vehicle 2 at time t.

$v_1(t)$: the speed of vehicle 1 at time t.

$v_2(t)$: the speed of vehicle 2 at time t.

Δa: the changing threshold

a_{bias}: the asymmetry term with positive value for left turn and negative value for right turn

Output:

Whether the incentive check passes or not